


Hierarchy of entanglement renormalization and long-range entangled states

Meng-Yuan Li and Peng Ye ^{*}

School of Physics, State Key Laboratory of Optoelectronic Materials and Technologies, and Guangdong Provincial Key Laboratory of Magnetoelectric Physics and Devices, Sun Yat-sen University, Guangzhou 510275, China



(Received 28 December 2022; revised 16 March 2023; accepted 20 March 2023; published 30 March 2023)

As a quantum-informative window into quantum many-body physics, the concept and application of the entanglement renormalization group (ERG) have been playing a vital role in the study of novel quantum phases of matter, especially long-range entangled (LRE) states in topologically ordered systems. For instance, by recursively applying local unitaries as well as adding and removing qubits that form product states, the 2D toric code ground states, i.e., the fixed point of \mathbb{Z}_2 topological order, are efficiently coarse-grained with respect to the system size. As a further improvement, the addition and removal of 2D toric codes in the ground states of the 3D X-cube model is shown to be indispensable and, remarkably, leads to well-defined fixed points of a large class of fracton orders that are non-liquid-like. Here, we present a substantially unified ERG framework in which general degrees of freedom are allowed to be recursively added or removed. Specifically, we establish an exotic hierarchy of ERG and LRE states in Pauli stabilizer codes, where the 2D toric code and 3D X-cube models are naturally included. In the hierarchy, LRE states like 3D X-cube and 3D toric code ground states can be added or removed in ERG processes of more complex LRE states. In this way, a large group of Pauli stabilizer codes are categorized into a series of state towers; within each tower, in addition to local unitaries including CNOT (controlled-NOT) gates, lower LRE states of level- n are added or removed in the level- n ERG process of an upper LRE state of level $(n + 1)$, connecting LRE states of different levels and unveiling complex relations among LRE states. As future directions, we expect this hierarchy can be applied to more general LRE states, leading to a unified ERG scenario of LRE states and exact tensor-network representations in the form of more generalized branching multiscale entanglement renormalization ansatz.

DOI: [10.1103/PhysRevB.107.115169](https://doi.org/10.1103/PhysRevB.107.115169)

I. INTRODUCTION

For the past few decades, the goal of classification and characterization of quantum phases of matter has been indispensably intertwined with surprisingly rapid progress on many-body quantum entanglement [1–16]. This line of effort significantly reshapes modern many-body physics from the emphasis of entanglement structure instead of local correlation functions and local order parameters. For instance, the topologically ordered ground states of, e.g., fractional quantum Hall liquids [17], chiral spin liquids [18], the toric code [19], and string-net models [20] have been identified as long-range entangled (LRE) states [9] that cannot be adiabatically connected to (unentangled) product states by local unitary (LU) transformations, i.e., disentanglers. In contrast, short-range entangled states (SRE) can always be connected to product states by LU transformations. In particular, symmetry-protected topological states (SPTs) [21], e.g., the Haldane spin chain, are a special class of SRE states in which all above-mentioned LU transformations inevitably break the global symmetry that protects SPT order. Remarkably, a series of stabilizer code models realizing topological orders are found to be fixed points of certain entanglement renormalization group (ERG) transformations

[4,5,7] that simultaneously lead to an efficient representation of the topologically ordered ground state in terms of a tensor network, the multiscale entanglement renormalization ansatz (MERA) [6–8]. The idea of ERG provides a remarkable quantum-informative framework that significantly revolutionizes the traditional real-space and momentum-space renormalization-group treatments of quantum many-body systems and quantum field theory. More specifically, during the process of ERG transformations, LU transformations and the addition and removal of product states are recursively performed, such that the number of qubits (i.e., the system size) and short-range entanglement can be coarse-grained while the long-range entanglement patterns (e.g., braiding and fusion data of 2D anyon systems) stay unaltered.

Recently, the concept of ERG transformations has been substantially advanced to unveil the quantum entanglement structure and fixed points of *fracton orders*—an exotic class of topologically ordered nonliquids [22–33]. In contrast to pure topological orders (e.g., the fractional quantum Hall states) that are liquid states, fracton orders are a kind of non-liquid-like LRE states whose local Hamiltonians support ground state degeneracy (GSD) that not only is locally indistinguishable (thus topologically ordered) but also grows subextensively with respect to the system size. For example, the GSD of X-cube model—the prototypical example of type-I fracton order—on a 3-torus satisfies that $\log_2 \text{GSD}$ grows linearly with the linear system size L [34]. Immediately, it has

^{*}yepeng5@mail.sysu.edu.cn

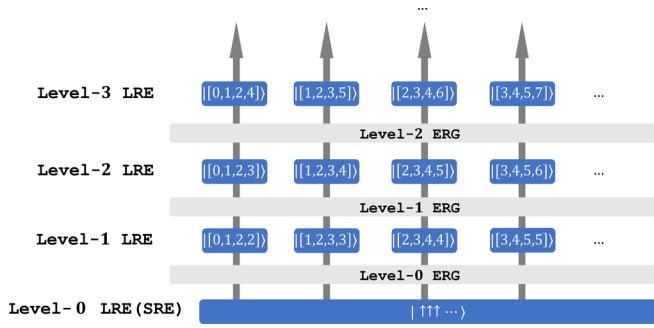


FIG. 1. Illustration of state towers that exhibit a hierarchy of entanglement renormalization and long-range entangled states. For concreteness, a class of Pauli stabilizer codes are studied, each of which is labeled by four integers. $[0,1,2,2]$, $[1,2,3,3]$, and $[0,1,2,3]$ are, respectively, 2D toric code, 3D toric code and 3D X-cube models. $|\cdot\rangle$ refers to a ground state of a certain model (i.e., a state in the stabilizer subspace, see Appendix B). There are a series of state towers denoted by upward arrows, and along each arrow a lower LRE^n state can be added or removed in the ERG^n process of the upper LRE^{n+1} state as demonstrated in Eq. (1). To unify the notation, SRE states (including unentangled product states) are symbolically denoted as LRE^0 .

been discovered that, to consistently define quantum phases and fixed points of fracton orders in the framework of entanglement renormalization, not only product states (i.e., SRE states) but also pure topological orders (i.e., a kind of LRE states) defined on lower dimensional space should be added or removed, such that two X-cube ground states of different system sizes can be adiabatically connected [22]. Despite the success of such ERG generalization, whether or not there is a much deeper mechanism towards a unified ERG framework is yet to be investigated.

In this paper, through exactly solvable models, we present a unified ERG framework via a hierarchical structure of ERG as well as the associated LRE states, where the above ERG transformations of original definition [4,5,7] and that of the X-cube model [22] are naturally included. To be more specific, as shown in Fig. 1, we construct ERG transformations for a series of Pauli stabilizer code models [35] proposed in Ref. [36], such that the models are fixed points of ERG transformations. All models we will study in this paper are uniquely denoted by four integers, i.e., $[d_n, d_s, d_l, D]$, where a subset labeled by $[d, d+1, d+2, D]$ is found to be a Pauli stabilizer code model with emergent \mathbb{Z}_2 gauge symmetry (see Sec. II for more details). The familiar 3D X-cube model is denoted as $[0,1,2,3]$. We also successfully incorporate toric code models of all dimensions into the labeling system, which has not been included in Ref. [36]. For example, the 2D toric code model is labeled by $[0,1,2,2]$. Remarkably, in the ERG transformations of these Pauli stabilizer codes, we find a hierarchical structure summarized in Fig. 1: In an ERG transformation connecting two $[d, d+1, d+2, D]$ states (i.e., the ground states of $[d, d+1, d+2, D]$ model as lattice Hamiltonian) with $D > d+2$ of different sizes, $[d, d+1, d+2, D-1]$ states are added or removed in addition to local unitaries (e.g., CNOT), such that all Pauli stabilizer codes are fixed points of the ERG transformations. While the \log_2 GSD of these topological nonliquid models grows polynomially with

respect to the linear system size [37], such ERG transformations are found to keep the GSD formulas consistent in different length scales. All in all, the ERG relation can be symbolically expressed as follows: $|[d, d+1, d+2, D]\rangle \sim |[d, d+1, d+2, D]\rangle' \otimes |[d, d+1, d+2, D-1]\rangle$, where $|[d, d+1, d+2, D]\rangle$ and $|[d, d+1, d+2, D]\rangle'$ are $[d, d+1, d+2, D]$ states of different sizes, and \sim means the two sides can be connected by an LU transformation.

In the unified framework, ERG transformations obey the following rules:

(1) In the ERG transformations on Pauli stabilizer codes considered here, LRE states are categorized into different levels, denoted as LRE^n with the level index $n = 0, 1, 2, \dots$. Unentangled product states and more general SRE states are dubbed level-0 LRE states (denoted as LRE^0 symbolically) for the notational convenience.

(2) ERG transformations where level- n LRE states are added or removed are dubbed level- n ERG (denoted as ERG^n symbolically) transformations. Unless otherwise specified, n is the highest level of added or removed LRE states;

(3) States of the same stabilizer code with different sizes that can be connected by level- n ERG transformations are identified as LRE^{n+1} .

Then an ERG^n transformation can be symbolically expressed as follows:

$$\text{ERG}^n : \text{LRE}^{n+1} \sim \text{LRE}^{n+1} \otimes \text{LRE}^n, \quad (1)$$

which explicitly shows a hierarchy of ERG transformations as well as LRE states along each upward arrow in Fig. 1. For example, the ERG of the 2D toric code is given by ERG^0 [4,5,7,14]:

$$\text{ERG}^0 : \text{LRE}^1 \sim \text{LRE}^1 \otimes \text{LRE}^0, \quad (2)$$

where a toric code ground state is denoted as LRE^1 and product states denoted as LRE^0 are added or removed (note that SRE states are also symbolically denoted as LRE^0 for notational convenience). Similarly, the ERG of the 3D X-cube model is given by ERG^1 [22]:

$$\text{ERG}^1 : \text{LRE}^2 \sim \text{LRE}^2 \otimes \text{LRE}^1, \quad (3)$$

where an X-cube ground state is denoted as LRE^2 and the 2D toric code ground state LRE^1 is added or removed.

We also note that the above rules are established in the concrete stabilizer codes studied in this paper. In fact, Eq. (1) may be, in principle, a concrete realization of the following more general level- m ERG transformation denoted as ERG^m :

$$\text{ERG}^m : \text{LRE}^n \sim \text{LRE}^n \otimes \text{LRE}^m, \quad (4)$$

where $m < n$ is generally required. Assuming the existence of such ERG^m transformations, a natural conjecture is that the level of LRE states may be decided by the ERG^m transformations of the highest possible level. We leave such general ERG transformations as well as implied MERAs to further exploration.

The reminder of this paper is organized as follows. In Sec. II, we introduce some very useful geometric notations used in this paper and give a brief introduction to the $[d, d+1, d+2, D]$ models that include the 2D toric code model and

the 3D X-cube model as special examples. Especially, we explain how to incorporate toric codes into the labeling system. Section III is dedicated to a detailed demonstration of some concrete ERG transformations. In Sec. III A, as a warm-up, we perform the ERG transformations on the 2D toric code model (denoted as $[0,1,2,2]$), while an alternative approach was reviewed in Appendix D by following Ref. [14]. In Sec. III B, we review the ERG transformations on the 3D X-cube model (denoted as $[0,1,2,3]$). Then, we concretely construct the ERG transformations of different levels for $[0,1,2,4]$ and $[1,2,3,4]$ models, respectively, in Secs. III C and III D. Section IV is dedicated to ERG transformations in general $[d, d+1, d+2, D]$ models. In Sec. IV A, we demonstrate a general recipe for the ERG transformations of general $[d, d+1, d+2, D]$ models. In Sec. IV B, we prove that the models are indeed fixed points of corresponding ERG transformations. Then, we demonstrate how these ERG transformations lead to the concept of a hierarchy of ERG transformations and LRE states in Sec. IV C. A summary and outlook is given in Sec. V.

II. LABELING SYSTEM OF PAULI STABILIZER CODES

This section is dedicated to the introduction of some backgrounds, including geometric notations and a family of Pauli stabilizer code models denoted by $[d, d+1, d+2, D]$. We especially notice that $[D-2, D-1, D, D]$ models can be regarded as a D -dimensional generalization of the 2D toric code model.

A. Geometric notations and lattice Hamiltonians

In this paper, we need to involve some discussion about high dimensional geometric objects, so we believe it is beneficial to first introduce some relevant notations. For the hypercubic lattice discussed in this paper, unless otherwise specified, we set the lattice constant to be 1. Then, we introduce the concept of n -cubes denoted by γ_n , that simply refers to n -dimensional analogs of a cube. For example, a γ_0 (0-cube) is simply a vertex, a γ_1 (1-cube) is a link, a γ_2 (2-cube) is a plaquette, and a γ_3 (3-cube) is a conventional cube. In a D -dimensional hypercubic lattice, with the above notations, we can use the coordinates of the center of a γ_n ($n \leq D$ is assumed) to refer to the γ_n itself, as such a γ_n can be uniquely determined by the coordinates. In addition, we can see that the coordinate representation of a γ_n in a D -dimensional hypercubic lattice is always composed of n half-odd integers (or half integer in shorthand) and $(D-n)$ integers. For example, in a 3D cubic lattice, the coordinate representation of a γ_2 (i.e., plaquette), such as $(\frac{1}{2}, \frac{1}{2}, 0)$ and $(\frac{7}{2}, 5, \frac{1}{2})$, always contains *two* half integers and *one* integer. What's more, following the terminology in Ref. [36], we say an n -cube $\gamma_n = (x_1, x_2, \dots, x_D)$ and an m -cube $\gamma_m = (y_1, y_2, \dots, y_D)$ to be nearest to each other when $|x_1 - y_1| + |x_2 - y_2| + \dots + |x_D - y_D| = \frac{|m-n|}{2}$ for $m \neq n$. Specially, when $m = n$, we say they are nearest to each other when $|x_1 - y_1| + |x_2 - y_2| + \dots + |x_D - y_D| = 1$. We can check that such a definition of being nearest is consistent with the usual conventions.

Next, we give a brief review of the definition of $[d, d+1, d+2, D]$ Pauli stabilizer code models. As lattice

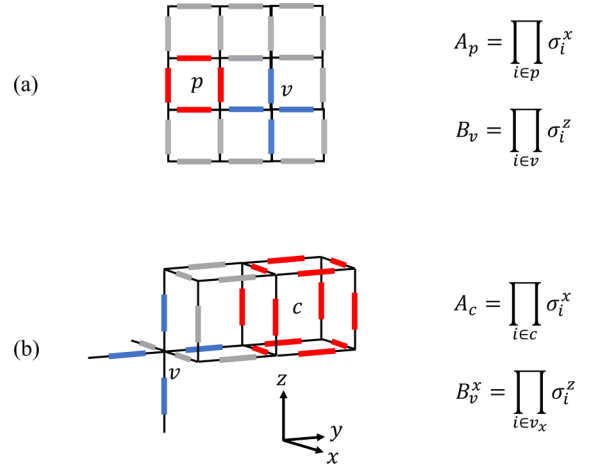


FIG. 2. Hamiltonians of some representative $[d, d+1, d+2, D]$ models. (a) and (b), respectively, demonstrate the Hamiltonian terms of the $[0,1,2,2]$ (2D toric code) and the $[0,1,2,3]$ (3D X-cube) model. In each subfigure, spins are represented by bars on links (aka γ_1 's), and we draw spins acted by an A term with red, and spins acted by a B term with blue. As we can see, in $[0,1,2,2]$ and $[0,1,2,3]$ models, A terms are, respectively, defined on plaquettes (aka γ_2 's) and cubes (aka γ_3 's). In (b), we only draw a single B_v^x term on vertex (aka γ_0) v that is composed of the four spins that are not only nearest to vertex v but also located in a plane perpendicular to \hat{x} direction. Such four spins are denoted as $i \in v_x$ in (b).

Hamiltonians, $[d, d+1, d+2, D]$ models is a subset of $[d_n, d_s, d_l, D]$ models proposed in Ref. [36]. In general, a $[d_n, d_s, d_l, D]$ model is defined on a D -dimensional hypercubic lattice, with one $\frac{1}{2}$ -spin defined on each d_s -cube (i.e., γ_{d_s}). And the Hamiltonian is given as follows:

$$H_{[d_n, d_s, d_l, D]} = - \sum_{\gamma_D} A_{\gamma_D} - \sum_{\gamma_{d_n}} \sum_l B_{\gamma_{d_n}}^l, \quad (5)$$

where a $B_{\gamma_{d_n}}^l$ term is the product of the z components of the spins (a) being nearest to the d_n -cube γ_{d_n} and (b) living in a d_l -dimensional subsystem given by index l , and an A_{γ_D} term is the product of the x components of the spins being nearest to the D -cube γ_D . Here for simplicity, all coefficients of terms have been set to be -1 . The ground states of the $[d, d+1, d+2, D]$ subset of models can be obtained in a similar manner as for the 2D toric code model (see Appendix B). Some concrete examples of model Hamiltonians are illustrated in Fig. 2. In Ref. [36], $d_n < d_s < d_l < D$ is assumed, while in this paper, we allow the case $d_l = D$ to give a more complete picture of the hierarchy of ERG transformations and LRE states. More details of this case are given in Sec. II B.

B. Incorporating toric codes

In this paper, we primarily focus on $[d, d+1, d+2, D]$ models (i.e., we set $d_n = d, d_s = d+1, d_l = d+2$). Here, we notice that 2D and 3D toric code models can also be included into the above model series as $[0,1,2,2]$ and $[1,2,3,3]$ models, respectively. In fact, generally a $[D-2, D-1, D, D]$ model can be recognized as a D -dimensional generalization of 2D toric code model. Here, because $[D-2, D-1, D, D]$

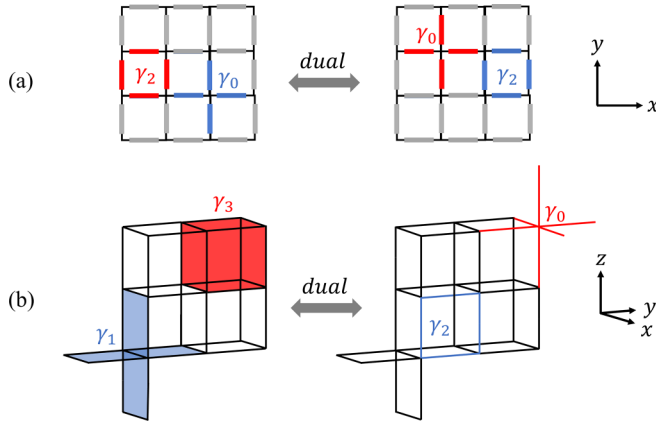


FIG. 3. Duality of $[0,1,2,2]$ and $[1,2,3,3]$ models. Here we show two examples of the duality between original $[D-2, D-1, D, D]$ models (on left-hand side) and corresponding dual models (on right-hand side). (a) and (b), respectively, demonstrate the duality of $[0,1,2,2]$ and $[1,2,3,3]$ models. In (a), the spins are defined on links (i.e., γ_1 's) on both sides, thus we use bars on links to refer to spins; an A_{γ_2} Hamiltonian term highlighted with red originally defined on a plaquette (i.e., γ_2) is mapped to an A_v term defined on a vertex (i.e., γ_0), and a B_{γ_0} term highlighted with blue originally defined on a vertex is mapped to a B_p term defined on a plaquette. In (b), the spins are, respectively, defined on plaquettes in the original model and links in the dual model, thus we do not explicitly show all the spins for clarity; an A_{γ_3} Hamiltonian term highlighted with red originally defined on a cube (i.e., γ_3) is mapped to an A_v term defined on a vertex, and a B_{γ_1} term highlighted with blue originally defined on a link is mapped to a B_p term defined on a plaquette.

models do not satisfy the $d_l < D$ condition, now the superscripts of B terms are redundant and a $B_{\gamma_{D-2}}$ term is simply the product of the z components of the four spins nearest to the γ_{D-2} .

To see the equivalence between a $[D-2, D-1, D, D]$ model and a D -dimensional toric code model, we can consider a duality, where γ_n 's are mapped to γ_{D-n} 's, that can be concretely realized by shifting the coordinates of all γ_n 's by $(\frac{1}{2}, \frac{1}{2}, \dots, \frac{1}{2})$. For a given $[D-2, D-1, D, D]$ model, upon the duality, we obtain a dual model that is still defined on a D -dimensional hypercubic lattice, but $\frac{1}{2}$ -spins originally defined on γ_{D-1} 's are now defined on γ_1 's (aka links). As for the Hamiltonian terms, the original A_{γ_D} terms defined on γ_D 's are mapped to A_v terms defined on γ_0 's (aka vertices), and the original $B_{\gamma_{D-2}}$ terms defined on γ_{D-2} 's are mapped to B_p terms defined on γ_2 's (aka plaquettes).

In summary, the Hamiltonian of the dual model defined on a D -dimensional hypercubic lattice is given by $H_{\text{dual}} = -\sum_v A_v - \sum_p B_p$, where each link is assigned with a $\frac{1}{2}$ -spin, A_v is the product of x components of spins nearest to the vertex v , B_p is the product of z components of spins nearest to the plaquette p (see Fig. 3 for the pictorial demonstration of some examples). Such a Hamiltonian is a D -dimensional generalization of the 2D toric code model [38], and the ground states of which are regarded as LRE¹ states realized in different spatial dimensions (i.e., D). Note that the dual models themselves are not a part of $[d, d+1, d+2, D]$ models, thus in this paper the original $[D-2, D-1, D, D]$ models are more involved.

III. HIERARCHY OF ERG TRANSFORMATIONS AND LRE STATES

In this section, we concretely demonstrate the ERG transformations of some $[d, d+1, d+2, D]$ states. First, in Secs. III A and III B, we perform the ERG transformations of $[0,1,2,2]$ (2D toric code) and $[0,1,2,3]$ (3D X-cube) models, respectively. Then, in Secs. III C and III D, we, respectively, construct the ERG transformations of $[0,1,2,4]$ and $[1,2,3,4]$ models.

A. Level-0 ERG transformation of $[0,1,2,2]$ (2D toric code) states

The ERG transformations of $[0,1,2,2]$ states have been proposed and studied previously [5,7,14]; see the review in Appendix D. For consistency, here we perform an ERG⁰ transformation of $[0,1,2,2]$ states in an explicitly different way. This alternative ERG process is very useful for designing ERG transformations of other $[d, d+1, d+2, D]$ models to be discussed in this paper.

First, we give an intuitive picture of the $[0,1,2,2]$ states based on the general discussion in Appendix B. In the $[0,1,2,2]$ (aka 2D toric code) model, spins are located at links of a 2D square lattice. In a superposed configuration of a $[0,1,2,2]$ state, a B_j term requires that vertex j can only have zero, two, or four flipped nearest spins, thus flipped spins must form closed strings. An A_i term flips the four spins on the links of plaquette i , thus contractible closed strings can freely fluctuate in a ground state. We will see that the ERG transformation indeed preserves this closed strings pattern of $[0,1,2,2]$ states.

We start with a ground state $|\xi_i\rangle$ of the $[0,1,2,2]$ model defined on a square lattice of the size $L_x \times L_y$ with periodic boundary condition (PBCs), and obtain a ground state $|\xi_f\rangle$ on a square lattice of the size $L_x \times (L_y + 1)$ with PBCs by the following transformations:

First, we choose a T^1 1-torus, aka loop) composed of the centers of parallel links along direction \hat{y} with the same \hat{y} coordinate, and regard the T^1 as a cut: All links intersecting with the T^1 are cut into two links. Without loss of generality, we assume the T^1 is located at $y = \frac{1}{2}$, which means the cut links are of the form $(i, \frac{1}{2})$, where i are integers. After that, we apply a rescaling. For each cut link $l = (i, \frac{1}{2})$, we double the length of l to 2. Then, we can see that l is cut into links $l_1 = (i, \frac{1}{2})$ and $l_2 = (i, \frac{3}{2})$ of length 1, and now the cut T^1 is located at $y = 1$. We assign the original spin on l to l_1 .

Second, for each l_2 , we put an additional spin of the state $|0\rangle$ on it. It means that we enlarge the Hilbert space by taking the tensor product of the original one and the added spins, and add a series of $-\sigma_{l_2}^z$ terms to the Hamiltonian to make all the added spins in the state $|0\rangle$ (since a term $-\sigma_{l_2}^z$ requires a ground state $|\phi\rangle$ to satisfy $\sigma_{l_2}^z|\phi\rangle = |\phi\rangle$). Then, for each original cut link l , we apply a CNOT (controlled-NOT) gate with the original qubit on l_1 as control qubit and the added one on l_2 as target [see Fig. 4(b)]. By conjugate action of CNOT gates, the added $-\sigma_{l_2}^z$ terms are mapped to $-\sigma_{l_1}^z \sigma_{l_2}^z$ terms (see Appendix A). As a result, given a cut link l , for an arbitrary Ising configuration $|\dots \sigma_l \dots\rangle$ from $|\xi_i\rangle$ ($\sigma_l = 0$ or 1), we have $|\dots \sigma_l \dots\rangle \rightarrow |\dots \sigma_l \sigma_l \dots\rangle$, where $\sigma_{l_1} = \sigma_{l_2} = \sigma_l$. The ground state transformed by steps above is denoted as $|\xi_1\rangle$.

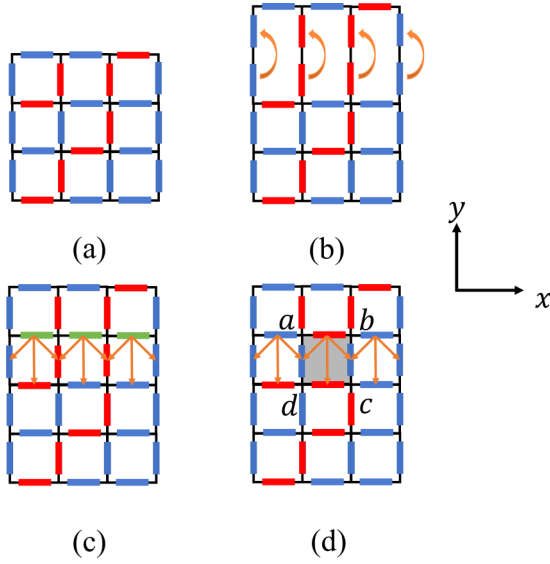


FIG. 4. ERG transformation of the 2D toric code model labeled by $[0,1,2,2]$. This ERG transformation is denoted as ERG^0 in Eq. (2). In (a), a closed string configuration in the original lattice is illustrated, where $|0\rangle$ spins on the links are denoted by blue bars, and $|1\rangle$ spins forming strings are highlighted with red. In (b), we illustrate the string configuration after the addition of spins in state $|0\rangle$, and the added spins *have been* transformed by CNOT gates such that the strings (formed by $|1\rangle$ spins) are still closed. These CNOT gates targeting on the additional spins are denoted by orange arrows pointing from control qubits to target qubits. In (c), we show the inserted $|\xi_p\rangle$ state and the CNOT gates applied on $|\xi_2\rangle$, where added spins of state $|\rightarrow\rangle$ are denoted by green bars and CNOT gates are also denoted by orange arrows. In (d), we illustrate an Ising configuration of $|\xi_f\rangle$, where a concrete configuration of $|\xi_p\rangle$ is picked, and the target spins have been correspondingly transformed by the CNOT gates. We can see that in such a configuration, flipped spins also form closed strings. In addition, an assignment of labels to the four vertices around a shadowed plaquette is also presented.

Third, we insert a product state $|\xi_p\rangle = |\rightarrow\rightarrow\rightarrow\cdots\rangle$ of size L_x on the cut T^1 given in the first step, where $|\rightarrow\rangle = \frac{1}{\sqrt{2}}(|0\rangle + |1\rangle)$ is the eigenstate of σ^x with eigenvalue 1. That is to say, the spins composing the inserted state are located on links of the form $(i + \frac{1}{2}, 1)$ in the rescaled lattice [see Fig. 4(c), note that there are no spins on such links before this step]. Then, we denote the tensor product of $|\xi_1\rangle$ and $|\xi_p\rangle$ as $|\xi_2\rangle = |\xi_1\rangle \otimes |\xi_p\rangle$.

Finally, we act a series of CNOT gates on $|\xi_2\rangle$ as illustrated in Figs. 4(c) and 4(d). The CNOT gates are organized in a translational invariant manner, thus we only need to specify them for a specific plaquette. Without loss of generality, we take $\gamma_2 = (\frac{1}{2}, \frac{1}{2})$ and denote the vertices of γ_2 by letters as shown in Fig. 4(d). Concretely, we have $d = (0, 0)$, $c = (1, 0)$, $a = (0, 1)$, and $b = (1, 1)$. Then, the CNOT gates can be explicitly specified as follows:

$$\sigma_{ab} \rightarrow \sigma_{bc}, \sigma_{cd}, \sigma_{da},$$

where σ_{xy} refers to the spin located on the link between x and y vertices, \rightarrow points from the control qubit to target qubits.

We can straightforwardly check that after the application of the CNOT gates on $|\xi_2\rangle$, we obtain $|\xi_f\rangle$ that preserves the

closed strings pattern of $[0,1,2,2]$ states. To see this, we show that the by conjugate action, the CNOT gates generate all stabilizer generators we need to obtain $[0,1,2,2]$ states on the enlarged lattice. First, by regarding $|\xi_p\rangle$ as stabilized by a series of σ^x stabilizers with $y = 1$ (i.e., for each σ^x stabilizer, the link where the stabilizer is defined satisfies $y = 1$), under the conjugate action of CNOT gates, a σ^x stabilizer with $y = 1$ is mapped to an A term with $y = \frac{1}{2}$; then, a $\sigma_{l_1}^z \sigma_{l_2}^z$ stabilizer obtained in the second step above is mapped to a B term with $y = 1$; finally, as we can note that also in the second step above, an A term with $y = \frac{1}{2}$ in the original lattice is mapped to a six-spin term composed of the x components of all spins around a modified A term and an A term with $y = \frac{1}{2}$, an arbitrary A term with $y = \frac{3}{2}$ can be obtained. Therefore, the $|\xi_f\rangle$ is indeed a $[0,1,2,2]$ state on the enlarged lattice. Or, from another perspective, the $[0,1,2,2]$ model is a fixed point of the ERG^0 transformation, as symbolically expressed in Eq. (2).

B. Level-1 ERG transformation of $[0,1,2,3]$ (3D X-cube) states

In this subsection, we review the ERG^1 transformation of the $[0,1,2,3]$ states following the recipe in Ref. [22]. Again, we first give an intuitive picture of the $[0,1,2,3]$ states based on the general discussion in Appendix B. In $[0,1,2,3]$ (aka 3D X-cube) model, spins are located at links of a 3D cubic lattice. In this case, $3 B_j^l$ terms with perpendicular l , where l denotes a plane containing vertex j , require j can only emanate three perpendicular strings composed of flipped spins; see Fig. 5(a). Intuitively, string configurations satisfying such constraints can be recognized as being composed of “cages” [39] in a manifold with trivial topology. An A_i term flips the 12 spins on the links of cube i , that can be regarded as forming a basic cage, thus such cages can freely fluctuate in a ground state. We will see that the ERG transformation indeed preserves this cage-net pattern of $[0,1,2,3]$ states.

We start with a ground state $|\xi_i\rangle$ of the $[0,1,2,3]$ model defined on a cubic lattice of size $L_x \times L_y \times L_z$ with PBCs, and obtain a ground state $|\xi_f\rangle$ on a cubic lattice of the size $L_x \times L_y \times (L_z + 1)$ with PBCs by the following transformations:

First, we choose a T^2 (2-torus) composed of the centers of parallel links along direction \hat{z} with the same \hat{z} coordinate, and regard the T^2 as a cut: All links intersecting with the T^2 are cut into two links. Without loss of generality, we assume the T^2 is located at $z = \frac{1}{2}$, which means the cut links are of the form $(i, j, \frac{1}{2})$, where i, j are integers. After that, we apply a rescaling. For each cut link $l = (i, j, \frac{1}{2})$, we double the length of l to 2. Then, we can see that l is cut into links $l_1 = (i, j, \frac{1}{2})$ and $l_2 = (i, j, \frac{3}{2})$ of length 1, and now the cut T^2 is located at $z = 1$. We assign the original spin on l to l_1 .

Second, for each l_2 , we put an additional spin of state $|0\rangle$ on it. It means that we enlarge the Hilbert space by taking the tensor product of the original one and the added spins, and add a series of $-\sigma_{l_2}^z$ terms to the Hamiltonian to make all the added spins in the state $|0\rangle$. Then, for each original cut link l , we apply a CNOT gate with the original qubit on l_1 as control qubit and the added one on l_2 as target. By conjugate action of CNOT gates, the added $-\sigma_{l_2}^z$ terms are mapped to $-\sigma_{l_1}^z \sigma_{l_2}^z$

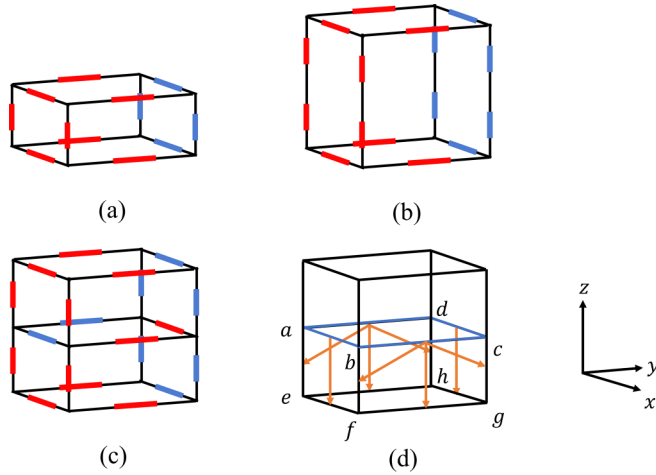


FIG. 5. ERG transformation of the 3D X-cube model labeled by $[0,1,2,3]$. This ERG transformation is denoted as ERG^1 in Eq. (3). We use red bars to denote spins occupied by strings in a configuration, and blue bars for the unoccupied ones. In (a), we demonstrate a configuration around the cube $\gamma_3 = (\frac{1}{2}, \frac{1}{2}, \frac{1}{2})$ in the original $|\xi_i\rangle$ state. In (b), we demonstrate the configuration obtained by cutting links of the form $(i, j, \frac{1}{2})$, rescaling the cut links, adding additional spins and applying a series of CNOT gates (i.e., a configuration from $|\xi_1\rangle$). In (c), we demonstrate a configuration after further inserting a $[0,1,2,2]$ (2D toric code) state $|\xi_{\text{gs}}\rangle$ (i.e., a configuration from $|\xi_2\rangle = |\xi_1\rangle \otimes |\xi_{\text{gs}}\rangle$). In (d), we demonstrate the CNOT gates applied on $|\xi_2\rangle$. Here, we use a different notation for clarity. The control qubits, i.e., spins from the inserted $[0,1,2,2]$ state on plane $z = 1$ (in the rescaled lattice), are denoted by blue links, while other spins are denoted by black links. The orange arrows point from control qubits to corresponding target qubits. Some vertices are denoted by letters.

terms (see Appendix A). As a result, given a cut link l , for an arbitrary Ising configuration $|\cdots \sigma_l \cdots\rangle$ from $|\xi_i\rangle$ ($\sigma_l = 0$ or 1), we have $|\cdots \sigma_l \cdots\rangle \rightarrow |\cdots \sigma_l \sigma_{l_2} \cdots\rangle$, where $\sigma_{l_1} = \sigma_{l_2} = \sigma_l$ [see Fig. 5(b)]. The ground state transformed by steps above is denoted as $|\xi_1\rangle$.

Third, we insert a $[0,1,2,2]$ (2D toric code) state $|\xi_{\text{gs}}\rangle$ of the size $L_x \times L_y$ on the cut T^2 given in the first step. That is to say, the spins composing the inserted state are located on links of the form $(i + \frac{1}{2}, j, 1)$ and $(i, j + \frac{1}{2}, 1)$ in the rescaled lattice [see Fig. 5(c), note that there are no spins on such links before this step]. Then, we denote the tensor product of $|\xi_1\rangle$ and $|\xi_{\text{gs}}\rangle$ as $|\xi_2\rangle = |\xi_1\rangle \otimes |\xi_{\text{gs}}\rangle$. As $[0,1,2,2]$ (2D toric code) model on a T^2 is fourfold degenerated, this step has four possible outcomes corresponding to four possible inserted $[0,1,2,2]$ states.

Finally, we act a series of CNOT gates on $|\xi_2\rangle$ as illustrated in Fig. 5(d). The CNOT gates are organized in a translational invariant manner, thus we only need to specify them for a specific cube. Without loss of generality, we take $\gamma_3 = (\frac{1}{2}, \frac{1}{2}, \frac{1}{2})$ and denote the vertices of γ_3 by letters as shown in Fig. 5(d). For example, we have $e = (0, 0, 0)$ and $c = (1, 1, 1)$. Then, the CNOT gates can be explicitly specified as follows:

$$\begin{aligned} \sigma_{bc} &\rightarrow \sigma_{bf}, \sigma_{cg}, \sigma_{fg}, \\ \sigma_{ad} &\rightarrow \sigma_{ae}, \sigma_{dh}, \sigma_{eh}, \\ \sigma_{ab} &\rightarrow \sigma_{ef}, \\ \sigma_{dc} &\rightarrow \sigma_{hg}, \end{aligned}$$

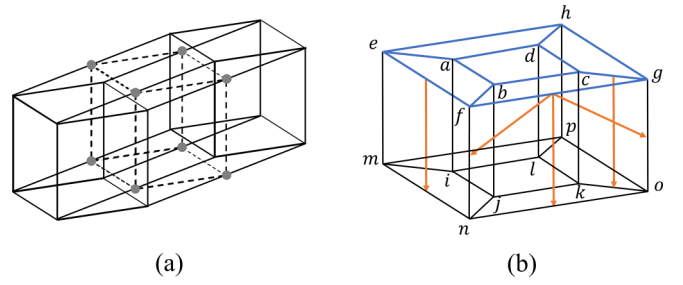


FIG. 6. ERG transformation of the $[0,1,2,4]$ model. In (a), we give a schematic picture of a 4-cube cut by a T^3 , where the intersection of the T^3 and the original 4-cube is denoted by the dashed 3-cube; for clarity, the intersection of the T^3 and corresponding links are denoted by gray dots. In (b), we demonstrate the CNOT gates applied on $|\xi_2\rangle$ following the same rules as in Fig. 5(d), while we use another way to illustrate the 4-cube to show the CNOT gates more clearly; here, we use blue links to denote control qubits from the inserted $[0,1,2,3]$ (3D X-cube) state on the cut T^3 with $x_4 = 1$ and black links for the target qubits. For simplicity, orange arrows pointing from control qubits to target qubits are only presented for three control qubits along different directions. As we can see, these CNOT gates satisfy all conditions given in the general recipe in Sec. IV B.

where σ_{xy} refers to the spin located on the link between x and y vertices, \rightarrow points from the control qubit to target qubits. Intuitively, we can see that by conjugate action (see Appendix A), the CNOT gates map the $A_p = \sigma_{ab}^x \sigma_{bc}^x \sigma_{cd}^x \sigma_{da}^x$ stabilizer of the inserted $[0,1,2,2]$ state to $A_c = \sigma_{ab}^x \sigma_{bc}^x \sigma_{cd}^x \sigma_{da}^x \sigma_{ef}^x \sigma_{fg}^x \sigma_{gh}^x \sigma_{he}^x \sigma_{ae}^x \sigma_{bf}^x \sigma_{cg}^x \sigma_{dh}^x$ that is a stabilizer of the $[0,1,2,3]$ (3D X-cube) state. Similarly, we can check that the CNOT gates generate all stabilizer generators we need to obtain $[0,1,2,3]$ states on a lattice of the size $L_x \times L_y \times (L_z + 1)$ with PBCs (see Sec. IV B for a more detailed demonstration).

Therefore, after the application of the CNOT gates on $|\xi_2\rangle$, we obtain $|\xi_f\rangle$, which is a ground state of $[0,1,2,3]$ (3D X-cube) model on a lattice of the size $L_x \times L_y \times (L_z + 1)$ with PBC. Pictorially, we can see the transformed state preserves the cage-net pattern of $[0,1,2,3]$ states.

Due to the fact that there are four possible choices of $|\xi_{\text{gs}}\rangle$ in the third step, for a given $|\xi_i\rangle$, we have four possible $|\xi_f\rangle$ outcomes. As a result, if we require the GSD formula to be symmetric for L_x , L_y , and L_z , the GSD of $[0,1,2,3]$ model has to satisfy $\log_2 \text{GSD} = 2L_x + 2L_y + 2L_z + C$, where C is a constant. This result is consistent with the exact result given in Ref. [34,37]. In addition, based on this method to obtain the GSD, it has been shown in Ref. [22] that the coefficients of linear terms in the \log_2 GSD are directly related to the topology of the 2D subsystems (dubbed as leaves) of $[0,1,2,3]$ model.

C. Level-2 ERG transformation of $[0,1,2,4]$ states

In this subsection, we demonstrate the ERG^2 transformation of $[0,1,2,4]$ states, with some essential steps pictorially shown in Fig. 6. Similar to the $[0,1,2,3]$ model, here we give an intuitive picture of $[0,1,2,4]$ states based on the general discussion in Appendix B. In the $[0,1,2,4]$ model, spins are located at links of a 4D hypercubic lattice. In this case, $6 B_j^l$

terms with perpendicular l , where l denotes a plane containing vertex j , require j can only emanate four perpendicular strings composed of flipped spins. An A_i term flips the 32 spins on the links of hypercube i . Similar to the cage-net pattern of [0,1,2,3] states [39], if we regard the links of a 4D hypercube as forming a 4D analog of a cage, we can intuitively understand the pattern of [0,1,2,4] states as where such 4D analogs of cage can freely fluctuate. We will see that the ERG transformation indeed preserves the pattern of [0,1,2,4] states.

Again, we start with a ground state $|\xi_i\rangle$ of the [0,1,2,4] model defined on a lattice of the size $L_1 \times L_2 \times L_3 \times L_4$ with PBCs and obtain a ground state $|\xi_f\rangle$ on a lattice of the size $L_1 \times L_2 \times L_3 \times (L_4 + 1)$ with PBCs. The ERG² transformation can be described as follows:

First, we choose a T^3 (3-torus) composed of the centers of parallel links along direction \hat{x}_4 with the same \hat{x}_4 coordinate and regard the T^3 as a cut: All links intersecting with the T^3 are cut into two links [see Fig. 6(a)]. Without loss of generality, we assume the T^3 is located at $x_4 = \frac{1}{2}$, which means the cut links are of the form $(i, j, k, \frac{1}{2})$, where i, j, k are integers. After that, we apply a rescaling. For each cut link $l = (i, j, k, \frac{1}{2})$, we double the length of l to 2. Then, we can see that l is cut into links $l_1 = (i, j, k, \frac{1}{2})$ and $l_2 = (i, j, k, \frac{3}{2})$ of length 1, and now the cut T^3 is located at $x_4 = 1$. We assign the original spin on l to l_1 .

Second, for each l_2 , we put an additional spin of the state $|0\rangle$ on it. It means that we enlarge the Hilbert space by taking the tensor product of the original one and the added spins and add a series of $-\sigma_l^z$ terms to the Hamiltonian to make all the added spins in state $|0\rangle$. Then, for each original cut link l , we apply a CNOT gate with the original qubit on l_1 as control qubit and the added one on l_2 as target. By conjugate action of CNOT gates, the added $-\sigma_l^z$ terms are mapped to $-\sigma_{l_1}^z \sigma_{l_2}^z$ terms (see Appendix A). As a result, given a cut link l , for an arbitrary Ising configuration $|\dots \sigma_l \dots\rangle$ from $|\xi_i\rangle$ ($\sigma_l = 0$ or 1), we have $|\dots \sigma_l \dots\rangle \rightarrow |\dots \sigma_{l_1} \sigma_{l_2} \dots\rangle$, where $\sigma_{l_1} = \sigma_{l_2} = \sigma_l$. The ground state transformed by the steps above is denoted as $|\xi_1\rangle$.

Third, we insert a [0,1,2,3] (3D X-cube) state $|\xi_{gs}\rangle$ of the size $L_1 \times L_2 \times L_3$ on the cut T^3 given in the first step. That is to say, the spins composing the inserted state are located on links of the form $(i + \frac{1}{2}, j, k, 1)$, $(i, j + \frac{1}{2}, k, 1)$, and $(i, j, k + \frac{1}{2}, 1)$ in the rescaled lattice (note that there are no spins on such links before this step). Then, we denote the tensor product of $|\xi_1\rangle$ and $|\xi_{gs}\rangle$ as $|\xi_2\rangle = |\xi_1\rangle \otimes |\xi_{gs}\rangle$. As the [0,1,2,3] (3D X-cube) model on the T^3 satisfies $\log_2 \text{GSD} = 2L_1 + 2L_2 + 2L_3 - 3$, this step has $2^{2L_1 + 2L_2 + 2L_3 - 3}$ possible outcomes corresponding to $2^{2L_1 + 2L_2 + 2L_3 - 3}$ possible inserted [0,1,2,3] states.

Finally, we act a series of CNOT gates on $|\xi_2\rangle$ as illustrated in Fig. 6(b). The CNOT gates are organized in a translational invariant manner, thus we only need to specify them for a specific 4-cube. Without loss of generality, we take $\gamma_4 = (\frac{1}{2}, \frac{1}{2}, \frac{1}{2}, \frac{1}{2})$ and denote the vertices of γ_4 by letters as shown in Fig. 6. Then, the CNOT gates can be explicitly specified as follows:

$$\begin{aligned} \sigma_{fg} &\rightarrow \sigma_{fn}, \sigma_{no}, \sigma_{og}, \\ \sigma_{bc} &\rightarrow \sigma_{bj}, \sigma_{jk}, \sigma_{kc}, \end{aligned}$$

$$\begin{aligned} \sigma_{ad} &\rightarrow \sigma_{ai}, \sigma_{il}, \sigma_{ld}, \\ \sigma_{eh} &\rightarrow \sigma_{em}, \sigma_{mp}, \sigma_{ph}, \\ \sigma_{ef} &\rightarrow \sigma_{mn}, \\ \sigma_{ab} &\rightarrow \sigma_{ij}, \\ \sigma_{dc} &\rightarrow \sigma_{lk}, \\ \sigma_{hg} &\rightarrow \sigma_{po}, \\ \sigma_{cg} &\rightarrow \sigma_{ko}, \\ \sigma_{bf} &\rightarrow \sigma_{jn}, \\ \sigma_{ae} &\rightarrow \sigma_{im}, \\ \sigma_{dh} &\rightarrow \sigma_{lp}, \end{aligned}$$

where σ_{xy} refers to the spin located on the link between x and y vertices; \rightarrow points from the control qubit to target qubits. Intuitively, we can see that by conjugate action (see Appendix A), the CNOT gates map the

$$A_c = \sigma_{ab}^x \sigma_{bc}^x \sigma_{cd}^x \sigma_{da}^x \sigma_{ae}^x \sigma_{bf}^x \sigma_{cg}^x \sigma_{dh}^x \sigma_{ef}^x \sigma_{fg}^x \sigma_{gh}^x \sigma_{he}^x$$

stabilizer of the inserted [0,1,2,3] state to

$$\begin{aligned} A_{\gamma_4} &= \sigma_{ab}^x \sigma_{bc}^x \sigma_{cd}^x \sigma_{da}^x \sigma_{ae}^x \sigma_{bf}^x \sigma_{cg}^x \sigma_{dh}^x \sigma_{ef}^x \sigma_{fg}^x \sigma_{gh}^x \sigma_{he}^x \sigma_{ij}^x \sigma_{jk}^x \sigma_{kl}^x \sigma_{li}^x \\ &\quad \times \sigma_{im}^x \sigma_{jn}^x \sigma_{ko}^x \sigma_{lp}^x \sigma_{mn}^x \sigma_{no}^x \sigma_{op}^x \sigma_{pm}^x \sigma_{ai}^x \sigma_{bj}^x \sigma_{ck}^x \sigma_{dl}^x \sigma_{em}^x \sigma_{fn}^x \sigma_{go}^x \sigma_{hp}^x \end{aligned}$$

that is a stabilizer of [0,1,2,4] ground state. Similarly, we can check that the CNOT gates generate all stabilizer generators we need to obtain [0,1,2,4] ground states on a lattice of size $L_1 \times L_2 \times L_3 \times (L_4 + 1)$ with PBCs (see Sec. IV B for a more detailed demonstration). Therefore, after the application of the CNOT gates on $|\xi_2\rangle$, we obtain $|\xi_f\rangle$, which is a ground state of [0,1,2,4] model on a lattice of size $L_1 \times L_2 \times L_3 \times (L_4 + 1)$ with PBCs.

Similar to the [0,1,2,3] model, we can see that the GSD of [0,1,2,4] model has to satisfy $\log_2 \text{GSD} = (2L_1 + 2L_2 + 2L_3 - 3)L_4 + C(L_1, L_2, L_3)$, where $C(L_1, L_2, L_3)$ is a function of L_1, L_2 and L_3 . When we require the GSD formula to be symmetric for L_1, L_2, L_3 and L_4 , then we have $\log_2 \text{GSD} = 2L_1 L_2 + 2L_1 L_3 + 2L_1 L_4 + 2L_2 L_3 + 2L_2 L_4 + 2L_3 L_4 - 3L_1 - 3L_2 - 3L_3 - 3L_4 + C'$, where C' is a constant. This result is consistent with the result obtained by ground state decomposition in Ref. [37].

D. Level-1 ERG transformation of [1,2,3,4] states

For comparison, in this subsection, we demonstrate the ERG¹ transformation of [1,2,3,4] states, with some essential steps pictorially shown in Fig. 7. We will see that, though the [1,2,3,4] model has the same spatial dimension as the [0,1,2,4] model, in the ERG transformation of its ground states, we only need to add or remove LRE¹ rather than LRE² states. Before the demonstration, here we also give an intuitive picture of [1,2,3,4] states based on the general discussion in Appendix B. In the [1,2,3,4] model, spins are located at plaquettes of a 4D hypercubic lattice. In this case, three B_j^l terms with perpendicular l , where l denotes a 3D subsystem containing link j , require j can only emanate three perpendicular membranes composed of flipped spins. An A_i term flips the 24 spins on the plaquettes of hypercube i . Again, similar to the cage-net pattern of [0,1,2,3] states [39], if we regard the plaquettes of a

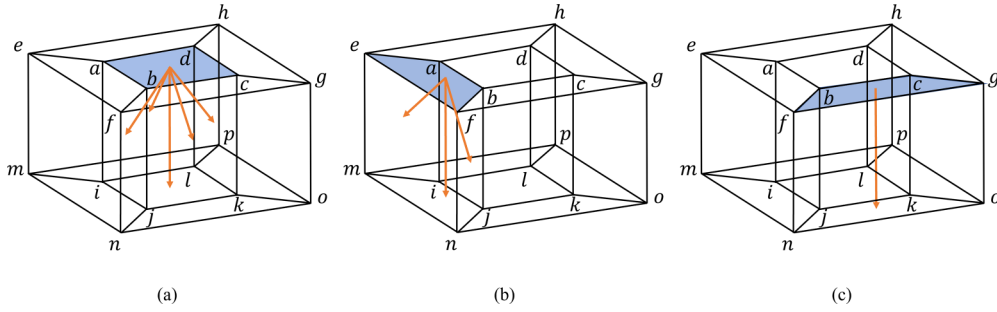


FIG. 7. ERG transformation of the [1,2,3,4] model. Here we follow a similar notation as in Fig. 6(b) to demonstrate the CNOT gates applied on $|\xi_2\rangle$. Again, we set qubits nearest to the cube specified by $abcdefgh$ as from the inserted [1,2,3,3] (3D toric code) state on the cut T^3 with $x_4 = 1$. For clarity, here we only demonstrate three control qubits and their associated CNOT gates. In (a)–(c), we use three transparent plaquettes highlighted with blue to denote three different control qubits and present orange arrows pointing from control qubits to target ones. Here it should be noticed that two different plaquettes may share the same center in these pictures, like $abcd$ and $efgh$. As we can see, these CNOT gates satisfy all conditions given in the general recipe in Sec. IV B.

4D hypercube as forming a 4D analog of a cage (note that the 4D analog here is different from the case of [0,1,2,4] states), we can intuitively understand the pattern of [1,2,3,4] states as where such 4D analogs of cage can freely fluctuate. We will see that the ERG transformation indeed preserves the pattern of [1,2,3,4] states.

Again, we start with a ground state $|\xi_i\rangle$ of the [1,2,3,4] model defined on a lattice of size $L_1 \times L_2 \times L_3 \times L_4$ with PBCs and obtain such a ground state $|\xi_f\rangle$ on a lattice of size $L_1 \times L_2 \times L_3 \times (L_4 + 1)$ with PBCs. The ERG¹ transformation can be similarly described as follows:

First, we choose a T^3 (3-torus) composed of the centers of parallel links along direction \hat{x}_4 with the same \hat{x}_4 coordinate and regard the T^3 as a cut: All plaquettes intersecting with the T^3 are cut into two plaquettes. Without loss of generality, we assume the T^3 is located at $x_4 = \frac{1}{2}$, which means the cut plaquettes are of the form $(i, j, k, \frac{1}{2}) + \frac{1}{2}I_n$, where $n = 1, 2, 3$, I_n is the unit vector along the \hat{x}_n direction, i, j, k are integers. After that, we apply a rescaling. For each cut plaquette $p = (i, j, k, \frac{1}{2}) + \frac{1}{2}I_n$, we double the linear size of p along the \hat{x}_4 direction to 2. Then, we can see that p is cut into plaquettes $p_1 = (i, j, k, \frac{1}{2}) + \frac{1}{2}I_n$ and $p_2 = (i, j, k, \frac{3}{2}) + \frac{1}{2}I_n$ with linear sizes along \hat{x}_4 direction equal to 1, and now the cut T^3 is located at $x_4 = 1$. We can assign the original spin on p to p_1 .

Second, for each p_2 , we put an additional spin of state $|0\rangle$ on it. Equivalently, it means that we enlarge the Hilbert space by taking the tensor product of the original one and the added spins, and add a series of $-\sigma_{p_2}^z$ terms to the Hamiltonian to make all the added spins in state $|0\rangle$. Then, for each original cut plaquette p , we apply a CNOT gate with the original qubit on p_1 as the control qubit and the added one on p_2 as the target. By conjugate action of CNOT gates, the added $-\sigma_{p_2}^z$ terms are mapped to $-\sigma_{p_1}^z \sigma_{p_2}^z$ terms (see Appendix A). As a result, given a cut plaquette p , for an arbitrary Ising configuration $|\dots\sigma_p\dots\rangle$ from $|\xi_i\rangle$ ($\sigma_p = 0$ or 1), we have $|\dots\sigma_p\dots\rangle \rightarrow |\dots\sigma_{p_1}\sigma_{p_2}\dots\rangle$, where $\sigma_{p_1} = \sigma_{p_2} = \sigma_p$. The ground state transformed by the steps above is denoted as $|\xi_1\rangle$.

Third, we insert a [1,2,3,3] (3D toric code) state $|\xi_{gs}\rangle$ of size $L_1 \times L_2 \times L_3$ on the cut T^3 given in the first step. That is to say, the spins composing the inserted state are located on plaquettes of the form $(i + \frac{1}{2}, j + \frac{1}{2}, k, 1)$, $(i, j + \frac{1}{2}, k + \frac{1}{2}, 1)$, and $(i + \frac{1}{2}, j, k + \frac{1}{2}, 1)$ in the rescaled lattice

(note that there are no spins on such plaquettes before this step). Then, we denote the tensor product of $|\xi_1\rangle$ and $|\xi_{gs}\rangle$ as $|\xi_2\rangle = |\xi_1\rangle \otimes |\xi_{gs}\rangle$. As the [1,2,3,3] (3D toric code) model on the T^3 satisfies $\log_2 \text{GSD} = 3$ [38,40], this step has 2^3 possible outcomes corresponding to 2^3 possible inserted [1,2,3,3] states.

Finally, we act a series of CNOT gates on $|\xi_2\rangle$ as illustrated in Fig. 7. The CNOT gates are organized in a translational invariant manner, thus we only need to specify them for a specific 4-cube. Without loss of generality, we take $\gamma_4 = (\frac{1}{2}, \frac{1}{2}, \frac{1}{2}, \frac{1}{2})$ and denote the vertices of γ_4 by letters as shown in Fig. 7. Then, the CNOT gates can be explicitly specified as follows:

$$\begin{aligned} \sigma_{abcd} &\rightarrow \sigma_{ijkl}, \sigma_{abji}, \sigma_{bckj}, \sigma_{cdlk}, \sigma_{dail}, \\ \sigma_{efgh} &\rightarrow \sigma_{mnop}, \sigma_{efnm}, \sigma_{fgon}, \sigma_{ghpo}, \sigma_{hemp}, \\ \sigma_{abfe} &\rightarrow \sigma_{ijnm}, \sigma_{aemi}, \sigma_{bf nj}, \\ \sigma_{cdhg} &\rightarrow \sigma_{klpo}, \sigma_{dhpl}, \sigma_{cgok}, \\ \sigma_{bcgf} &\rightarrow \sigma_{jkon}, \\ \sigma_{daeh} &\rightarrow \sigma_{limp}, \end{aligned}$$

where σ_{xyzw} refers to the spin located on the plaquette between x, y, z , and w vertices; \rightarrow points from the control qubit to target qubits. Intuitively, we can see that by conjugate action (see Appendix A), the CNOT gates map the

$$A_c = \sigma_{abcd}^x \sigma_{efgh}^x \sigma_{abfe}^x \sigma_{bcgf}^x \sigma_{cdhg}^x \sigma_{daeh}^x$$

stabilizer of the inserted [1,2,3,3] state to

$$\begin{aligned} A_{\gamma_4} &= \sigma_{abcd}^x \sigma_{efgh}^x \sigma_{abfe}^x \sigma_{bcgf}^x \sigma_{cdhg}^x \sigma_{daeh}^x \\ &\times \sigma_{ijkl}^x \sigma_{mnop}^x \sigma_{ijnm}^x \sigma_{jkon}^x \sigma_{klpo}^x \sigma_{limp}^x \\ &\times \sigma_{aemi}^x \sigma_{bf nj}^x \sigma_{efnm}^x \sigma_{abji}^x \sigma_{bckj}^x \sigma_{fgon}^x \\ &\times \sigma_{cgok}^x \sigma_{dhpl}^x \sigma_{ghpo}^x \sigma_{cdlk}^x \sigma_{dail}^x \sigma_{hemp}^x, \end{aligned}$$

which is a stabilizer of [1,2,3,4] ground state. Similarly, we can check that the CNOT gates generate all stabilizer generators we need to obtain [1,2,3,4] ground states on a lattice of the size $L_1 \times L_2 \times L_3 \times (L_4 + 1)$ with PBC (see Sec. IV B for a more detailed demonstration). Therefore, after the application of the CNOT gates on $|\xi_2\rangle$, we obtain $|\xi_f\rangle$, which is a ground

state of [1,2,3,4] model on a lattice of the size $L_1 \times L_2 \times L_3 \times (L_4 + 1)$ with PBC.

Similar to [0,1,2,3] model, we can see that the GSD of [1,2,3,4] model has to satisfy $\log_2 \text{GSD} = 3 \times L_4 + C(L_1, L_2, L_3)$, where $C(L_1, L_2, L_3)$ is a function of L_1, L_2 and L_3 . When we require the GSD formula to be symmetric for L_1, L_2, L_3 and L_4 , then we have $\log_2 \text{GSD} = 3L_1 + 3L_2 + 3L_3 + 3L_4 + C'$, where C' is a constant. This result is consistent with the result obtained by ground state decomposition in Ref. [37].

IV. ERG OF GENERIC LEVELS

In this section, we first show a generic recipe of the construction of ERG^{D-d-2} transformations of $[d, d+1, d+2, D]$ models with $D > d+2$. After that, in Sec. IV B, we prove that for such a $[d, d+1, d+2, D]$ model, the constructed ERG transformation indeed gives ground states of the same model of different sizes, i.e., the models are fixed points of the corresponding ERG transformations. Finally, in Sec. IV C, we discuss the hierarchy of ERG transformations and LRE states based on the constructed ERG transformations. Note that ERG^0 transformations of $[D-2, D-1, D, D]$ models are not included in this recipe.

A. Level- $(D-d-2)$ ERG transformation of $[d, d+1, d+2, D]$ states

In general, for a $[d, d+1, d+2, D]$ model with $D > d+2$, we can demonstrate the ERG^{D-d-2} transformation of $[d, d+1, d+2, D]$ states. Again, we start with a ground state $|\xi_i\rangle$ of $[d, d+1, d+2, D]$ model defined on a lattice of size $L_1 \times L_2 \times \dots \times L_D$ with PBCs and obtain a ground state $|\xi_f\rangle$ on a lattice of size $L_1 \times L_2 \times \dots \times (L_D + 1)$ with PBCs. The ERG^{D-d-2} transformation can be described as follows:

(1) First, we choose a $(D-1)$ -torus T^{D-1} composed of the centers of links with the same \hat{x}_D coordinate. Without loss of generality, we set the chosen T^{D-1} to be located at $x_D = \frac{1}{2}$, such that it is composed of the centers of links of the form $(n_1, n_2, \dots, n_{D-1}, \frac{1}{2})$, where n_1, n_2, \dots, n_{D-1} are integers. Then we regard the T^{D-1} as a cut: Every γ_{d+1} intersecting with the T^{D-1} is cut into 2 γ_{d+1} 's with identical spins. That is to say, for each cut γ_{d+1} , we put an additional spin in state $|0\rangle$, and then apply a CNOT gate with the original qubit as control qubit and the added one as target. In consequence, given a cut γ_{d+1} , for an arbitrary Ising configuration $|\dots \sigma_{\gamma_{d+1}} \dots\rangle$ from $|\xi_i\rangle$ ($\sigma_{\gamma_{d+1}} = 0$ or 1), we have $|\dots \sigma_{\gamma_{d+1}} \dots\rangle \rightarrow |\dots \sigma_{(\gamma_{d+1})_1} \sigma_{(\gamma_{d+1})_2} \dots\rangle$, where $\sigma_{(\gamma_{d+1})_1} = \sigma_{(\gamma_{d+1})_2} = \sigma_{\gamma_{d+1}}$. Then, we rescale the lattice by extending the linear size of the cut γ_{d+1} along the \hat{x}_D direction to 2, such that now the chosen T^{D-1} is composed of sites of the form $(n_1, n_2, \dots, n_{D-1}, 1)$, and for a cut $\gamma_{d+1} = (\dots, \frac{1}{2})$ in the original lattice, the original and additional spins are, respectively, assigned to $(\gamma_{d+1})_1 = (\dots, \frac{1}{2})$ and $(\gamma_{d+1})_2 = (\dots, \frac{3}{2})$ in the rescaled lattice. The ground state transformed by this step is denoted as $|\xi_1\rangle$.

(2) Second, we put a $[d, d+1, d+2, D-1]$ ground state $|\xi_{\text{gs}}\rangle$ of size $L_1 \times \dots \times L_{D-1}$ on the T^{D-1} given in the previous step. That is to say, we can regard the $(n_1, n_2, \dots, n_{D-1}, 1)$ sites as forming a hypercubic lattice defined on the T^{D-1} , and consider a $[d, d+1, d+2, D-1]$

ground state $|\xi_{\text{gs}}\rangle$ defined on this lattice. Then, by taking the tensor product of $|\xi_1\rangle$ and $|\xi_{\text{gs}}\rangle$, we obtain $|\xi_2\rangle = |\xi_1\rangle \otimes |\xi_{\text{gs}}\rangle$.

(3) Third, we act an LU transformation \mathcal{U} composed of a series of CNOT gates on $|\xi_2\rangle$ (see Sec. IV B for a demonstration of this LU transformation \mathcal{U}). After that, we obtain $|\xi_f\rangle$, which is a ground state of the $[d, d+1, d+2, D]$ model on a lattice of the size $L_1 \times L_2 \times \dots \times (L_D + 1)$ with PBCs.

To see that this generic recipe is consistent with the GSD results obtained by ground-state decomposition in Ref. [37], without loss of generality, say that in the polynomial $\log_2 \text{GSD}$ of $[d, d+1, d+2, D-1]$ model on the T^{D-1} , the coefficient of $L_i L_j \dots L_n$ term is c (here $i < j < \dots < n < D$ is assumed). Then, the above ERG transformation requires that the number of copies of $c L_i L_j \dots L_n$ contained in the $\log_2 \text{GSD}$ of $[d, d+1, d+2, D]$ model grows linearly with L_D . That is to say, the polynomial $\log_2 \text{GSD}$ of the $[d, d+1, d+2, D]$ model has to contain the term $c L_i L_j \dots L_n L_D$. This result is consistent with the relevant results from Ref. [37].

B. $[d, d+1, d+2, D]$ models as fixed points of level- $(D-d-2)$ ERG transformations

In this subsection, we give the conditions that an LU transformation \mathcal{U} used in step 3 of the ERG^{D-d-2} transformation of a general $[d, d+1, d+2, D]$ state should satisfy, and prove that such an LU transformation \mathcal{U} indeed gives ground states of the $[d, d+1, d+2, D]$ model on a lattice of different sizes by considering the conjugate action of \mathcal{U} on the Hamiltonian terms. Without loss of generality, we assume the cut T^{D-1} is extended along $\hat{x}_1, \hat{x}_2, \dots, \hat{x}_{D-1}$ directions, and the location is given by $x_D = 1$ (in the rescaled lattice). For convenience, here we explicitly write the Hamiltonian of a $[d, d+1, d+2, D]$ model as below:

$$H_{[d, d+1, d+2, D]} = - \sum_{\gamma_D} A_{\gamma_D} - \sum_{\gamma_d} \sum_l B_{\gamma_d}^l, \quad (6)$$

where an A_{γ_D} term is the product of the x components of the $\binom{D}{d+1} \times 2^{D-d-1}$ spins nearest to the γ_D , a $B_{\gamma_d}^l$ term is the product of the z components of the four spins that are (a) nearest to the γ_d and (b) living in the $(d+2)$ -dimensional subsystem l .

We start with the conditions that the LU transformation \mathcal{U} should satisfy. According to the LU transformation \mathcal{U} of [0,1,2,3], [0,1,2,4], and [1,2,3,4] models (i.e., the CNOT gates applied on $|\xi_2\rangle$ states of corresponding subsections), we expect such an LU transformation in the ERG^{D-d-2} transformation of a general $[d, d+1, d+2, D]$ state to satisfy the following conditions:

(1) First, we require \mathcal{U} to be composed of a series of CNOT gates around γ_D 's with $x_D = \frac{1}{2}$, where all control qubits are from the cut T^{D-1} (i.e., being located on γ_{d+1} 's with $x_D = 1$). In addition, we require \mathcal{U} to be translational invariant, such that the application of the CNOT gates is the same for every applied γ_D . Therefore, we only need to consider the application of CNOT gates in a single γ_D to specify \mathcal{U} . Without loss of generality, we can focus on $\gamma_D^r = (\frac{1}{2}, \frac{1}{2}, \dots, \frac{1}{2})$. Here the superscript r is for reference.

(2) Second, for each γ_{d+1} in γ_D^r with $x_D = 0$, we require the qubit on it to be controlled by the qubit on $\gamma_{d+1} + I_D$,

where $I_D = (0, 0, \dots, 0, 1)$ is the unit vector along the \hat{x}_D direction. Obviously, the qubit on such a γ_{d+1} is only controlled by one control qubit in γ'_d .

(3) Third, for each γ_{d+1} in γ'_D with $x_D = \frac{1}{2}$, we require the qubit on it to be controlled by exactly one nearest control qubit in γ'_D . In addition, for a pair of nearest parallel qubits, we require them to be simultaneously controlled (or not) by the control qubit that links them. For example, a pair of nearest parallel qubits, respectively, defined on $(\underbrace{\frac{1}{2}, \frac{1}{2}, \dots, \frac{1}{2}}_d, \underbrace{0, 0, \dots, 0}_{D-d})$ and

$(\underbrace{\frac{1}{2}, \frac{1}{2}, \dots, \frac{1}{2}}_d, \underbrace{1, 0, \dots, 0}_{D-d})$ are either both controlled by

$(\underbrace{\frac{1}{2}, \frac{1}{2}, \dots, \frac{1}{2}}_d, \underbrace{\frac{1}{2}, 0, \dots, 0}_{D-d})$ or not (here we can notice that

this control qubit is the only one that links the pair, i.e., simultaneously being nearest to the pair of qubits).

The existence of such LU transformations is obvious. And we can check that when (a) $d = 0, D = 3$, (b) $d = 0, D = 4$, and (c) $d = 1, D = 4$, the LU transformations \mathcal{U} in the ERG transformations of $[0,1,2,3]$, $[0,1,2,4]$, and $[1,2,3,4]$ states all satisfy the above conditions. In addition, here we should notice that each target qubit σ_i with $x_D = \frac{1}{2}$ is always controlled by two qubits. Without loss of generality, say qubit σ_i on $(d+1)$ -cube $i = (\underbrace{\frac{1}{2}, \frac{1}{2}, \dots, \frac{1}{2}}_d, \underbrace{0, 0, \dots, 0}_{D-d})$ is controlled

by the qubit on $i_c = (\underbrace{\frac{1}{2}, \frac{1}{2}, \dots, \frac{1}{2}}_d, \underbrace{\frac{1}{2}, 0, \dots, 0}_{D-d})$, accord-

ing to the translational invariance of the LU transformation, the qubit on $i' = i - I_{d+1} = (\underbrace{\frac{1}{2}, \frac{1}{2}, \dots, \frac{1}{2}}_d, \underbrace{-1, 0, \dots, 0}_{D-d})$

must be controlled by the qubit on $i'_c = i_c - I_{d+1} = (\underbrace{\frac{1}{2}, \frac{1}{2}, \dots, \frac{1}{2}}_d, \underbrace{-\frac{1}{2}, 0, \dots, 0}_{D-d})$; after that, as i and i' are paral-

lel $(d+1)$ -cubes connected by i'_c , σ_i must also be controlled by the qubit on i'_c . Then, we can notice that an arbitrary γ_D nearest to i has the form $(\underbrace{\frac{1}{2}, \frac{1}{2}, \dots, \frac{1}{2}}_d, \underbrace{\pm\frac{1}{2}, \pm\frac{1}{2}, \dots, \pm\frac{1}{2}}_{D-d})$,

thus it must be either nearest to i_c or i'_c . Since a target qubit can only be controlled by one control qubit from a nearest γ_D as required by the conditions above, no other qubits in the T^{D-1} can control σ_i . In conclusion, for any target qubit σ_i with $x_D = \frac{1}{2}$, there are always two qubits that control it.

Then we show that though the concrete form of the LU transformation \mathcal{U} has not been specified, the above conditions can make sure that \mathcal{U} produces the ground states as expected. That is to say, for an LU transformation \mathcal{U} satisfying the conditions above, a $|\xi_f\rangle = \mathcal{U}|\xi_2\rangle$ is indeed a ground state of the $[d, d+1, d+2, D]$ model.

First, we notice that \mathcal{U} is applied on the $|\xi_2\rangle$ given in Sec. IV A, and $|\xi_2\rangle$ can be obtained as a ground state of the following Hamiltonian:

$$H_1 = H_{dddD} + H_{dddD-1} + H_{zz}, \quad (7)$$

where H_{dddD} refers to the terms in the original $[d, d+1, d+2, D]$ model with some modifications according to the cut γ_{d+1} 's (see below), H_{dddD-1} refers to the terms of the $[d, d+$

$1, d+2, D-1]$ Hamiltonian on the cut T^{D-1} , and $H_{zz} = -\sum_i \sigma_i^z \sigma_{i+I_D}^z$ is added to make each pair of spins on a cut γ_{d+1} identical, where i refers to a $(d+1)$ -cube with $x_D = \frac{1}{2}$ in the rescaled lattice. Note that the A_{γ_D} terms in H_{dddD} near the T^{D-1} are modified to $A'_{\gamma_D} = A_{\gamma_D} A_{\gamma_D+I_D}$ to be consistent with the cut γ_{d+1} 's, where A_{γ_D} and $A_{\gamma_D+I_D}$ have the same form as an ordinary A term from the original $[d, d+1, d+2, D]$ model, and γ_D satisfies $x_D = \frac{1}{2}$. As a concrete example, in the $[0,1,2,4]$ model, where $d = 0, D = 4$, such a modified A_{γ_4} , denoted as A'_{γ_4} , is given by $A'_{\frac{1}{2}, \frac{1}{2}, \frac{1}{2}, \frac{1}{2}} = A_{\frac{1}{2}, \frac{1}{2}, \frac{1}{2}, \frac{1}{2}} A_{\frac{1}{2}, \frac{1}{2}, \frac{1}{2}, \frac{3}{2}}$, where operators $A_{\frac{1}{2}, \frac{1}{2}, \frac{1}{2}, \frac{1}{2}}$ and $A_{\frac{1}{2}, \frac{1}{2}, \frac{1}{2}, \frac{3}{2}}$ themselves do not present in H_{dddD} . Furthermore, for a B_{γ_d} term from H_{dddD} with $x_D = 2$ that involves qubit σ_i with $x_D = \frac{1}{2}$, we can replace it by the product of the B term itself and a corresponding $\sigma_i^z \sigma_{i+I_D}^z$ term, such that σ_i^z in the B term is replaced by $\sigma_{i+I_D}^z$. This modification makes such B terms connected. For example, in the $[0,1,2,3]$ model, due to our assignment that for a cut link the original qubit is put on a link of the form $(\dots, \frac{1}{2})$, in the rescaled lattice, we would have B terms such as $B_{(0,0,2)}^z = \sigma_{(0, \frac{1}{2}, 2)}^z \sigma_{(0, -\frac{1}{2}, 2)}^z \sigma_{(0,0, \frac{5}{2})}^z \sigma_{(0,0, \frac{1}{2})}^z$, that is not connected, without such modifications. Similarly, we can freely add B_{γ_d} terms with $x_D = \frac{3}{2}$ to H_1 as such terms can be directly obtained by taking the products of B_{γ_d} terms with $x_D = \frac{1}{2}$ and corresponding $\sigma_i^z \sigma_{i+I_D}^z$ terms. In addition, H_{dddD} contains no B_{γ_d} terms on the T^{D-1} . After that, we can see that all terms in H_1 still commute with each other. From another perspective, H_1 can also be obtained by considering the conjugate action of the CNOT gates applied in the first step in Sec. IV A. A more detailed demonstration of the terms in H_1 is given in Appendix C.

Second, because the \mathcal{U} transformation is a product of a series of CNOT gates, the conjugate action of \mathcal{U} on an arbitrary stabilizer G can be reduced to the conjugate action of CNOT gates on G . With the general mapping rules given by the conjugate action of CNOT gates (see Appendix A), we can obtain all terms in the transformed Hamiltonian H_2 as follows:

(1) First, since for an arbitrary γ_{D-1} inside the T^{D-1} , all qubits that are controlled by the qubits from the γ_{D-1} together with the control qubits themselves form a γ_D with $x_D = \frac{1}{2}$, $A_{\gamma_{D-1}}$ terms in H_{dddD-1} are mapped to A_{γ_D} terms with $x_D = \frac{1}{2}$.

(2) Second, since an arbitrary target qubit σ_i with $x_D = \frac{1}{2}$ is controlled by exactly two qubits from the T^{D-1} , each $\sigma_i^z \sigma_{i+I_D}^z$ term in H_{zz} is mapped to a four-spin term composed of the original $\sigma_i^z, \sigma_{i+I_D}^z$ and the z components of the two qubits that control σ_i .

(3) Third, further considering that an arbitrary target qubit σ_i with $x_D = 0$ is only controlled by σ_{i+I_D} from the T^{D-1} , a B_{γ_d} term in H_{dddD} near the T^{D-1} should be modified as follows: (a) for a qubit σ_i with $x_D = 0$ involved in the B term, multiply the term by $\sigma_{i+I_D}^z$; (b) for a qubit σ_i with $x_D = \frac{1}{2}$ involved in the B term, multiply the term by the z components of the two qubits that control σ_i . As an example, for a B_{γ_d} term only involving qubits with $x_D = 0$, it is mapped to a $B_{\gamma_d} B_{\gamma_d+I_D}$ term, where $B_{\gamma_d+I_D}$ is obtained by adding I_D to the coordinates of all qubits involved in B_{γ_d} .

(4) Finally, all other terms stay invariant under the conjugate action of \mathcal{U} .

We denote the Hamiltonian of $[d, d + 1, d + 2, D]$ model on the lattice of size $L_1 \times L_2 \times \cdots \times (L_D + 1)$ with PBCs as H_3 [see Eq. (6)]. Then we can notice that by taking the product of A terms obtained in the first step and A' terms from H_{ddd} , we can obtain all A terms that exist in H_3 but superficially missing in H_2 ; by taking the product of the four-spin terms obtained in the second step (which can be recognized as B terms in H_3), modified B terms obtained in the third step and B terms in H_{ddd-1} , we can obtain all B terms that exist in H_3 but are superficially missing in H_2 . Therefore, all terms of H_3 can be obtained by taking the product of terms of H_2 (a more detailed demonstration is given in Appendix C). As is also straightforward to check the other way around, finally, we can see that H_2 and H_3 are equivalent Pauli stabilizer code models with equivalent stabilizer groups and $|\xi_f\rangle = \mathcal{U}|\xi_2\rangle$ is indeed a ground state of H_3 .

C. Discussions

As we have demonstrated in this section, in the ERG transformations of different $[d, d + 1, d + 2, D]$ states, the added or removed states are also different LRE states. In other words, the entanglement patterns in $[d, d + 1, d + 2, D]$ states with different D and a fixed d are intrinsically different, and these models cannot be fully understood as fixed points of a finite number of types of ERG transformations. Instead, we need an infinite series of ERG transformations of different levels to understand the more general long-range entanglement patterns.

Therefore, we conclude the above observations by proposing the concept of a hierarchy of ERG transformations, where each transformation is assigned with an integer level. Correspondingly, LRE states are assigned with integer levels as well (see Fig. 1). For a given stabilizer code model considered in this paper, two level- $(n + 1)$ LRE (LRE^{n+1}) states of different sizes can be connected by a level- n ERG (ERG^n) transformation, that is composed of LU transformations combined with addition or removal of level- n LRE states. Furthermore, if we define product states and SRE states as LRE^0 states, then we have $[0,1,2,2]$ (2D toric code) states as O states, $[0,1,2,3]$ (3D X-cube) states as LRE^2 states, $[0,1,2,4]$ states as LRE^3 states and so on. In addition, we can see that low level LRE states themselves can be recognized as trivial high-level LRE states, just like a product state is recognized as a trivial pure topological order. Especially, a decoupled stack of LRE^n states is also a trivial LRE^{n+1} state, as it can be reduced to nothing under a ERG^n transformation.

V. SUMMARY AND OUTLOOK

In this paper, by considering a class of Pauli stabilizer codes, we constructed a more unified ERG framework through adding and removing more general degrees of freedom. The well-established ERG processes of the $[0,1,2,2]$ (2D toric code) and $[0,1,2,3]$ (3D X-cube) model are naturally included as the simplest cases. All Pauli stabilizer codes considered here are categorized into a series of state towers as shown in Fig. 1; in each tower, lower LRE states of level n are added or removed in the level- n ERG process of an upper LRE state of level- $(n + 1)$. Several future directions are listed below.

First, we may expect a more general ERG framework shown in Eq. (4) can be constructed in other stabilizer codes.

Second, the completeness of the concept of level of LRE states needs further exploration. For example, for type-II fracton ordered states [34,41,42], such as Haah's code [41], a series of ERG transformations have been constructed and studied [23,24,26], nevertheless, whether it is possible to consistently assign a level to such type-II fracton ordered states and corresponding ERG transformations is yet to be determined. Some further discussion about the hierarchy of ERG transformations may be beneficial for a more complete understanding of the entanglement patterns in more generic fracton orders.

Third, except for the stabilizer code models considered in this paper, physically, we can also consider models perturbed by external fields, which are no longer exactly solvable. Constructing ERG transformations for such models to investigate their fixed points is also an interesting direction. And some numerical techniques may also be useful in the study of such models [43–45].

Finally, it is known that the ERG transformations are related to MERA, which is a kind of tensor network capable of efficiently encoding the entanglement signatures of certain quantum many-body states [6–8,46]. In Ref. [22], it has been noted that $[0,1,2,3]$ (3D X-cube) states bear exact branching MERA representations. Then it is natural to ask whether LRE states of general levels can have such tensor network representations. If so, the holographic geometries generated by such tensor networks are also worth exploring [47–49].

ACKNOWLEDGMENTS

This work was supported by NSFC Grant No. 12074438, Guangdong Basic and Applied Basic Research Foundation under Grant No. 2020B1515120100, and the Open Project of Guangdong Provincial Key Laboratory of Magnetoelectric Physics and Devices under Grant No. 2022B1212010008.

APPENDIX A: A BRIEF INTRODUCTION OF CONTROLLED-NOT CNOT GATE

Here we give a brief introduction of the CNOT gate that is frequently used in the main text of this paper.

By definition, a CNOT gate is a two-qubit unitary operation. In the σ^z basis, for $|x\rangle, |y\rangle$, where $x, y \in \{0, 1\}$, the CNOT gate maps $|x\rangle \otimes |y\rangle$ to $|x\rangle \otimes |y \oplus x\rangle$; here \otimes means tensor product, \oplus means modulo-2 addition. Effectively, the CNOT gate regards the first qubit as a *control qubit* and the second qubit as a *target qubit*. When the control (first) qubit is $|0\rangle$, then the CNOT gate does nothing; when the control qubit is $|1\rangle$, the CNOT gate flips the target (second) qubit, thus the name. For example, denoting the action of the CNOT gate as U , we have $U|01\rangle = |01\rangle$ and $U|11\rangle = |10\rangle$.

For the usage in the main text, here we also introduce the conjugate action of the CNOT gate on stabilizers (i.e., Hamiltonian terms of a stabilizer code model and their products). For a state $|\phi\rangle$ in the stabilizer subspace and a stabilizer G (i.e., $G|\phi\rangle = |\phi\rangle$), if we apply a CNOT gate U on $|\phi\rangle$, then we have $(UGU^\dagger)U|\phi\rangle = U|\phi\rangle$. That is to say, the transformed state $U|\phi\rangle$ is stabilized by UGU^\dagger , that is G acted by the conjugate

action of the CNOT gate. For a specific G acting nontrivially on some control or target qubits, the correspondence between G and UGU^\dagger can be expressed as follows [5,22]:

$$\begin{aligned} ZI &\rightarrow ZI, \\ IZ &\leftrightarrow ZZ, \\ XI &\leftrightarrow XX, \\ IX &\rightarrow IX, \end{aligned}$$

where the first qubit refers to the control qubit and the second qubit refers to the target qubit. For example, if we consider the conjugate action of a CNOT gate on a stabilizer G , where G applies a σ^x on the control qubit and applies an identity on the target qubit, then the corresponding UGU^\dagger will apply σ^x on both qubits.

APPENDIX B: GROUND STATE WAVE FUNCTIONS OF $[d, d+1, d+2, D]$ STABILIZER CODE MODELS

In this Appendix, we show a general recipe to obtain the ground states of $[d, d+1, d+2, D]$ stabilizer code models (including $[D-2, D-1, D, D]$ models, such as 2D and 3D toric codes) in a similar manner as in the distinguished 2D toric code model. The lattice Hamiltonians of $[d, d+1, d+2, D]$ models are all of the following form:

$$H = -\sum_i A_i - \sum_j B_j, \quad (\text{B1})$$

where i and j are some kinds of spatial locations (e.g., vertices, centers of links, and centers of plaquettes) depending on the specific model, and the index l in Eq. (5) has been formally absorbed into index j for simplicity. Here, A_i and B_j are, respectively, local products of σ^x and σ^z Pauli operators, and they all commute with each other (see Fig. 2 for examples of $[0,1,2,2]$ and $[0,1,2,3]$ models). Therefore, a ground state $|\phi\rangle$ of such a Hamiltonian has to satisfy constraints $A_i|\phi\rangle = |\phi\rangle$, $\forall i$ and $B_j|\phi\rangle = |\phi\rangle$, $\forall j$ (respectively denoted as A and B constraints). That is to say, for a given $[d, d+1, d+2, D]$ model, the A_i and B_j operators can be regarded as generators of a stabilizer group, and the ground state subspace is the corresponding stabilizer subspace [14,35], as ground states are stabilized by all A_i and B_j operators. In this paper, as we mainly care about the stabilizer subspaces, unless otherwise specified, for a given model, we only consider states in its ground state subspace. Then, for an arbitrary $[d, d+1, d+2, D]$ stabilizer code model, we can obtain a ground state $|\phi_n\rangle$ of it by the following procedures:

(1) First, we consider the σ^z basis, that is to say, we use Ising configurations, where spins are denoted by their direction along σ^z , as a basis of the whole Hilbert space. For a single qubit, we use the convention $\sigma^z|\uparrow\rangle = |\uparrow\rangle = |0\rangle = \begin{pmatrix} 1 \\ 0 \end{pmatrix}$, $\sigma^z|\downarrow\rangle = -|\downarrow\rangle = -|1\rangle = -\begin{pmatrix} 0 \\ 1 \end{pmatrix}$ (i.e., $|0\rangle$ for spin up, and $|1\rangle$ for spin down).

(2) Second, we can notice that $|0 \cdots 00\rangle$ naturally satisfies all B constraints. We denote $|0 \cdots 00\rangle$ as the reference state.

(3) Third, we consider the equal weight superposition of the reference state and all configurations that can be obtained by applying a series of A_i operators on the reference state, and denote this state as $|\phi_n\rangle$. As all A_i and B_j operators commute

with each other, $|\phi_n\rangle$ also satisfies B constraints. According to our construction of $|\phi_n\rangle$, where two configurations that can be related by the action of A_i are always equally superposed, we can see that $|\phi_n\rangle$ must also satisfy A constraints. Hence, $|\phi_n\rangle$ is a ground state of the stabilizer code model.

Similarly to the 2D toric code model, we use an intuitive picture to describe an Ising configuration by recognizing flipped spins (i.e., spin of the state $|1\rangle$) as occupied by certain geometric objects. For example, if the spins are defined on links, then we recognize flipped spins as occupied by strings; if the spins are defined on plaquettes, then we recognize flipped spins as occupied by membranes. For a $[d, d+1, d+2, D]$ model, other ground states can be obtained by applying logical operators on the $|\phi_n\rangle$ state. Here in the σ^z basis, a logical operator can be recognized as a product of a series of σ^x operators that commutes with all B_j terms and is not equivalent to any product of a series of A_i terms. For instance, in the $[0,1,2,2]$ model defined on a T^2 (2-torus), such a logical operator is a noncontractible closed string composed of σ^x operators [19].

Following this general recipe, we can see that when we ignore the topological degeneracy by focusing on the open boundary condition, we only need to consider the $|\phi_n\rangle$ state, which can be regarded as a superposition of a series of configurations. For the $|\phi_n\rangle$ state, B terms require a superposed configuration to satisfy certain constraints, like flipped spins forming closed strings in a $[0,1,2,2]$ model; A terms require configurations that can be connected by the action of A terms to be equal-weight superposed. In Sec. III, a series of concrete examples are demonstrated in the corresponding subsections.

APPENDIX C: PROOF OF THE EQUIVALENCE BETWEEN HAMILTONIANS H_2 AND H_3

In this Appendix, we concretely demonstrate that in Sec. IV B, all terms in H_3 , the Hamiltonian of $[d, d+1, d+2, D]$ model on the lattice of size $L_1 \times L_2 \times \cdots \times (L_D + 1)$ with PBCs, can be obtained by taking the product of terms in H_2 and vice versa, thus they are equivalent stabilizer code models. As we can notice that H_2 and H_3 only have different terms around the T^{D-1} with $x_D = 1$, we only need to consider terms defined on locations with $0 \leq x_D \leq 2$.

Before discussing terms in H_2 , we would like to give a detailed demonstration and classification of the terms around the cut T^{D-1} in $H_1 = H_{dddD} + H_{dddD-1} + H_{zz}$. Such terms in H_1 can be classified as follows:

- (1) BI terms: B terms with $x_D = 0$ from H_{dddD} that only involve qubits with $x_D = 0$.
- (2) BII terms: B terms with $x_D = 0$ from H_{dddD} that simultaneously involve qubits with $x_D = 0$ and $x_D = \frac{1}{2}$.
- (3) $BIII$ terms: B terms with $x_D = \frac{1}{2}$ from H_{dddD} .
- (4) BIV terms: B terms with $x_D = 1$ from H_{dddD-1} (i.e., such B terms only involve qubits with $x_D = 1$).
- (5) BV terms: B terms with $x_D = \frac{3}{2}$, 2 from H_{dddD} .
- (6) AI terms: $A'_{\gamma_D} = A_{\gamma_D} A_{\gamma_D + I_D}$ terms with $x_D = \frac{1}{2}$ from H_{dddD} .
- (7) AII terms: $A_{\gamma_{D-1}}$ terms with $x_D = 1$ from H_{dddD-1} .
- (8) C terms: $C_{\gamma_{d+1}} = \sigma_{\gamma_{d+1}}^z \sigma_{\gamma_{d+1} + I_D}^z$ with $x_D = \frac{1}{2}$ from H_{zz} .

We can notice that, around the T^{D-1} , H_3 is composed of BI , BII , $BIII$, BIV , BV , and the following terms:

(1) BVI terms: B terms with $x_D = 1$ that involve qubits with $x_D \neq 1$.

(2) $AIII$ terms: A_{γ_D} terms with $x_D = \frac{1}{2}, \frac{3}{2}$.

Then, we consider the conjugate action of the LU transformation \mathcal{U} on the terms in H_1 that leads to terms in H_2 (note that here the superscripts of B terms are omitted, as we only need to consider the types of terms):

(1) A BI term B_{γ_d} is mapped to $B_{\gamma_d}B_{\gamma_d+I_D}$, the product of the BI term itself and a BIV term $B_{\gamma_d+I_D}$.

(2) A BII term B_{γ_d} is mapped to (a) the BII term itself, if the qubits with $x_D = 0$ and $x_D = \frac{1}{2}$ in B_{γ_d} are controlled by the same pair of qubits from the T^{D-1} ; (b) $B_{\gamma_d}B_{\gamma_d+I_D}$, the product of the BII term itself and a BIV term $B_{\gamma_d+I_D}$, if otherwise.

(3) A $BIII$ term B_{γ_d} is mapped to (a) the $BIII$ term itself, if two perpendicular qubits in B_{γ_d} [i.e., the two qubits are nearest and from different $(d+1)$ -dimensional subsystems] share one control qubit; (b) $B_{\gamma_d}B_{\gamma_d^1}B_{\gamma_d^2}$, the product of the $BIII$ term itself and two BIV terms $B_{\gamma_d^1}$ and $B_{\gamma_d^2}$, if two perpendicular qubits in B_{γ_d} have control qubits nearest to the same γ_d ; (c) $B_{\gamma_d}B_{\gamma_d^1}B_{\gamma_d^2}B_{\gamma_d^3}B_{\gamma_d^4}$, the product of the $BIII$ term itself and four BIV terms $B_{\gamma_d^1}$, $B_{\gamma_d^2}$, $B_{\gamma_d^3}$, and $B_{\gamma_d^4}$, if otherwise;

(4) BIV , BV , AI terms stay invariant.

(5) An AII term $A_{\gamma_{D-1}}$ terms with $x_D = 1$ is mapped to an $AIII$ term A_{γ_D} with $x_D = \frac{1}{2}$, where the γ_D is obtained by $\gamma_D = \gamma_{D-1} - \frac{1}{2}I_D$.

(6) A C term $C_{\gamma_{d+1}}$ term is mapped to a BVI term B_{γ_d} with $x_D = 1$, where the γ_d is obtained as $\gamma_d = \gamma_{d+1} + \frac{1}{2}I_D$.

Because BIV , BV , AI terms are invariant under the conjugate action of \mathcal{U} (i.e., they present in H_2), we can obtain an arbitrary BI , BII , or $BIII$ term by taking the product of the corresponding transformed term with invariant BIV terms. An arbitrary $AIII$ term with $x_D = \frac{1}{2}$ can be obtained as a transformed AII term, and an arbitrary $AIII$ term with $x_D = \frac{3}{2}$ can be obtained by taking the product of a transformed AII term and an invariant AI term. In addition, by taking the product of a transformed C term with a BIV term, an arbitrary BVI term can also be obtained. Finally, because it is straightforward to check that all terms in H_2 can be obtained by taking products of terms in H_3 , as two stabilizer code models H_2 and H_3 have equivalent sets of stabilizer generators, thus the stabilizer subspaces should be equivalent.

APPENDIX D: ANOTHER LEVEL-0 ERG TRANSFORMATION OF $[0,1,2,2]$ STATES

In this Appendix, we review the ERG^0 transformation of $[0,1,2,2]$ (2D toric code) states following the recipe in Ref. [14]. In this 0 transformation of a $[0,1,2,2]$ state defined on a square lattice with PBC, we first separate vertices into A and B sublattices. Then, we put an additional $1/2$ -spin in state $|0\rangle$ on each vertex [see Fig. 8(a)]. After that, we apply an LU transformation \mathcal{U}_1 that is composed of a series of CNOT gates: For each additional spin, we act two CNOT gates targeting on it. More specifically, for an additional qubit in sublattice A, we use the qubits on the upper and left links as control

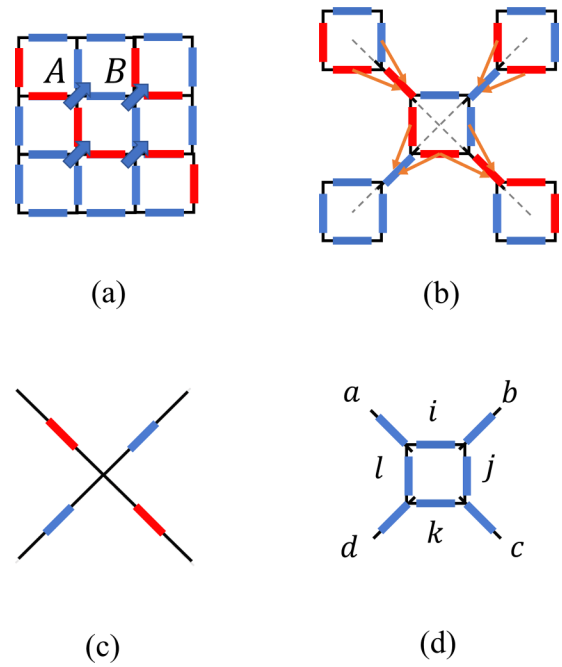


FIG. 8. Another ERG transformation of the 2D toric code model labeled by $[0,1,2,2]$. This ERG transformation is denoted as ERG^0 in Eq. (2). In (a), we demonstrate how the original vertices are separated into two sublattices. A closed string configuration is illustrated, where $|0\rangle$ spins on the links are denoted by blue bars, and $|1\rangle$ spins forming strings are highlighted with red. The four blue arrows on four vertices denote four additional spins in state $|0\rangle$. In (b), we can see the four vertices are now extended to four links connecting plaquettes, and their corresponding additional spins, which are also denoted by bars now, *have been* transformed by CNOT gates such that the strings (formed by $|1\rangle$ spins) are still closed. These CNOT gates targeting the four additional spins are denoted by orange arrows pointing from control qubits to target qubits. In addition, dashed lines connecting the centers of squares are presented. As we can see, the action of CNOT gates couples additional and original spins in a manner that indeed preserves the closed strings pattern of $[0,1,2,2]$ (2D toric code) state. By dropping all spins nearest to squares after another LU transformation, we obtain (c), in which a square lattice with a larger lattice constant appears and spins are located at the centers of new links [i.e., the dashed lines in (b)]. We can see that, now, spins on the centers of new links form a $[0,1,2,2]$ state on a new square lattice. In (d), we demonstrate an assignment of labels to the eight links around a square, where diagonal links are denoted by a , b , c , and d ; links nearest to the square are denoted by i , j , k , and l .

qubits; for an additional qubit in sublattice B, we use qubits on the upper and right links [see Fig. 8(b)]. The action of \mathcal{U}_1 can be understood pictorially: Recall that in any allowed Ising configuration of a $[0,1,2,2]$ state, there must be either an even number or zero of $|1\rangle$ spins around each vertex, thus flipped spins always form closed strings. Then we can notice that the design of CNOT gates in \mathcal{U}_1 exactly preserves this constraint by integrating additional spins into the closed strings pattern.

After that, we further apply an LU transformation \mathcal{U}_2 to map the spins around each square to $|0000\rangle + |1111\rangle$ (normalization is omitted), and such spins can be removed out of the

state as $|0000\rangle + |1111\rangle$ can be transformed to a product state by a LU operator. For the lattice, the LU transformation \mathcal{U}_2 and the removal of spins effectively shrinks every square to a vertex as shown in Fig. 8(c). By noticing that in each configuration there is always an even number or zero of diagonal links around each square with qubits in $|1\rangle$, the resulting state also has the closed strings pattern. Here, to see that \mathcal{U}_2 is indeed an LU transformation, we can recognize $\mathcal{U}_2 = \prod_s \mathcal{U}_s$, which is the product of \mathcal{U}_s operators supported around each square s . A \mathcal{U}_s acts on the four qubits on links nearest to the square s (denoted by i, j, k , and l) and the four qubits on the diagonal links around s [denoted by a, b, c , and d , see Fig. 8(d)]. Here, \mathcal{U}_s can be roughly recognized as a generalized CNOT gate: It takes the qubits on diagonal links as control qubits and qubits on the square as targets. For a specific configuration of the eight qubits, the action of \mathcal{U}_s can be obtained as follows: (a) if all control qubits are $|0\rangle$, then flip no target qubits; (b) if two control qubits are $|1\rangle$, then flip the target qubits between them clockwise following the alphabetical order (e.g., if qubits on b and d are $|1\rangle$, then flip qubits on j and k); (c) if all control qubits are in $|1\rangle$, then flip qubits on i and k . Then, \mathcal{U}_s obviously

satisfies $\mathcal{U}_s \mathcal{U}_s = \mathbb{I}$, thus $\mathcal{U}_s^{-1} = \mathcal{U}_s$. Next, notice that Ising configurations form a complete basis of the Hilbert space: For an arbitrary pair of Ising configurations of the eight qubits $|\psi_1\rangle$ and $|\psi_2\rangle$, we can obtain that $\langle \psi_1 | \mathcal{U}_s | \psi_2 \rangle = \langle \psi_2 | \mathcal{U}_s | \psi_1 \rangle^*$: We only have $\langle \psi_1 | \mathcal{U}_s | \psi_2 \rangle = 1$ when the control qubits in $|\psi_1\rangle$ and $|\psi_2\rangle$ are all the same, and only the qubits to be flipped are different in $|\psi_1\rangle$ and $|\psi_2\rangle$; otherwise, $\langle \psi_1 | \mathcal{U}_s | \psi_2 \rangle = 0$. As a result, $\mathcal{U}_s^\dagger = \mathcal{U}_s = \mathcal{U}_s^{-1}$, thus \mathcal{U}_s is both unitary and Hermitian. Since the transformations above do not change the pattern that the state is invariant under the action of A_p terms on squares, and \mathcal{U}_s always maps the configuration of a square to $|0000\rangle$ or $|1111\rangle$, we can see that spins nearest to each square are indeed mapped to $|0000\rangle + |1111\rangle$.

Finally, we obtain a $[0,1,2,2]$ state on a square lattice with a larger lattice constant. That is to say, after an ERG transformation composed of adding and removing product states and LU transformations, the structure of the $[0,1,2,2]$ state is preserved. Or, from another perspective, the $[0,1,2,2]$ model is a fixed point of the ERG⁰ transformation as symbolically expressed in Eq. (2). A pictorial demonstration of this ERG transformation is given in Fig. 8.

-
- [1] S. R. White, Density Matrix Formulation for Quantum Renormalization Groups, *Phys. Rev. Lett.* **69**, 2863 (1992).
- [2] S. R. White, Density-matrix algorithms for quantum renormalization groups, *Phys. Rev. B* **48**, 10345 (1993).
- [3] U. Schollwöck, The density-matrix renormalization group, *Rev. Mod. Phys.* **77**, 259 (2005).
- [4] G. Vidal, Entanglement Renormalization, *Phys. Rev. Lett.* **99**, 220405 (2007).
- [5] M. Aguado and G. Vidal, Entanglement Renormalization and Topological Order, *Phys. Rev. Lett.* **100**, 070404 (2008).
- [6] G. Vidal, Class of Quantum Many-body States That can be Efficiently Simulated, *Phys. Rev. Lett.* **101**, 110501 (2008).
- [7] R. König, B. W. Reichardt, and G. Vidal, Exact entanglement renormalization for string-net models, *Phys. Rev. B* **79**, 195123 (2009).
- [8] G. Evenbly and G. Vidal, Class of Highly Entangled Many-body States That can be Efficiently Simulated, *Phys. Rev. Lett.* **112**, 240502 (2014).
- [9] X. Chen, Z.-C. Gu, and X.-G. Wen, Local unitary transformation, long-range quantum entanglement, wave function renormalization, and topological order, *Phys. Rev. B* **82**, 155138 (2010).
- [10] M. Levin and X.-G. Wen, Detecting Topological Order in a Ground State Wave Function, *Phys. Rev. Lett.* **96**, 110405 (2006).
- [11] H. Li and F. D. M. Haldane, Entanglement Spectrum as a Generalization of Entanglement Entropy: Identification of Topological Order in Non-Abelian Fractional Quantum Hall Effect States, *Phys. Rev. Lett.* **101**, 010504 (2008).
- [12] A. Kitaev and J. Preskill, Topological Entanglement Entropy, *Phys. Rev. Lett.* **96**, 110404 (2006).
- [13] F. Pollmann, A. M. Turner, E. Berg, and M. Oshikawa, Entanglement spectrum of a topological phase in one dimension, *Phys. Rev. B* **81**, 064439 (2010).
- [14] B. Zeng, X. Chen, D.-L. Zhou, and X.-G. Wen, *Quantum Information Meets Quantum Matter*, Quantum Science and Technology (QST) (Springer, New York, 2019).
- [15] Z.-C. Gu and X.-G. Wen, Tensor-entanglement-filtering renormalization approach and symmetry-protected topological order, *Phys. Rev. B* **80**, 155131 (2009).
- [16] X.-G. Wen, Colloquium: Zoo of quantum-topological phases of matter, *Rev. Mod. Phys.* **89**, 041004 (2017).
- [17] S. M. Girvin, Introduction to the fractional quantum Hall effect, in *The Quantum Hall Effect*, edited by B. Douçot, V. Pasquier, B. Duplantier, and V. Rivasseau, Progress in Mathematical Physics book series (PMP), Vol. 45 (Birkhäuser, Basel, 2005), pp. 133–162.
- [18] X. G. Wen, Vacuum degeneracy of chiral spin states in compactified space, *Phys. Rev. B* **40**, 7387 (1989).
- [19] A. Kitaev, Anyons in an exactly solved model and beyond, *Ann. Phys.* **321**, 2 (2006).
- [20] M. A. Levin and X.-G. Wen, String-net condensation: A physical mechanism for topological phases, *Phys. Rev. B* **71**, 045110 (2005).
- [21] X. Chen, Z.-C. Gu, Z.-X. Liu, and X.-G. Wen, Symmetry-protected topological orders in interacting bosonic systems, *Science* **338**, 1604 (2012).
- [22] W. Shirley, K. Slagle, Z. Wang, and X. Chen, Fracton Models on General Three-Dimensional Manifolds, *Phys. Rev. X* **8**, 031051 (2018).
- [23] J. Haah, Bifurcation in entanglement renormalization group flow of a gapped spin model, *Phys. Rev. B* **89**, 075119 (2014).
- [24] B. Swingle and J. McGreevy, Renormalization group constructions of topological quantum liquids and beyond, *Phys. Rev. B* **93**, 045127 (2016).
- [25] B. Swingle and J. McGreevy, Mixed s-sourcery: Building many-body states using bubbles of nothing, *Phys. Rev. B* **94**, 155125 (2016).
- [26] A. Dua, P. Sarkar, D. J. Williamson, and M. Cheng, Bifurcating entanglement-renormalization group flows of fracton stabilizer models, *Phys. Rev. Res.* **2**, 033021 (2020).

- [27] W. Shirley, K. Slagle, and X. Chen, Foliated fracton order in the checkerboard model, *Phys. Rev. B* **99**, 115123 (2019).
- [28] T. Wang, W. Shirley, and X. Chen, Foliated fracton order in the Majorana checkerboard model, *Phys. Rev. B* **100**, 085127 (2019).
- [29] W. Shirley, X. Liu, and A. Dua, Emergent fermionic gauge theory and foliated fracton order in the Chamon model, *Phys. Rev. B* **107**, 035136 (2023).
- [30] X.-G. Wen, Systematic construction of gapped nonliquid states, *Phys. Rev. Res.* **2**, 033300 (2020).
- [31] J. Wang, Nonliquid cellular states: Gluing gauge-higher-symmetry-breaking versus gauge-higher-symmetry-extension interfacial defects, *Phys. Rev. Res.* **4**, 023258 (2022).
- [32] R. M. Nandkishore and M. Hermele, Fractons, *Annu. Rev. Condens. Matter Phys.* **10**, 295 (2019).
- [33] M. Pretko, X. Chen, and Y. You, Fracton phases of matter, *Int. J. Mod. Phys. A* **35**, 2030003 (2020).
- [34] S. Vijay, J. Haah, and L. Fu, Fracton topological order, generalized lattice gauge theory, and duality, *Phys. Rev. B* **94**, 235157 (2016).
- [35] D. Gottesman, Stabilizer codes and quantum error correction, Ph.D. thesis, California Institute of Technology, 1997.
- [36] M.-Y. Li and P. Ye, Fracton physics of spatially extended excitations, *Phys. Rev. B* **101**, 245134 (2020).
- [37] M.-Y. Li and P. Ye, Fracton physics of spatially extended excitations. II. Polynomial ground state degeneracy of exactly solvable models, *Phys. Rev. B* **104**, 235127 (2021).
- [38] A. Hamma, P. Zanardi, and X.-G. Wen, String and membrane condensation on three-dimensional lattices, *Phys. Rev. B* **72**, 035307 (2005).
- [39] A. Prem, S.-J. Huang, H. Song, and M. Hermele, Cage-net Fracton Models, *Phys. Rev. X* **9**, 021010 (2019).
- [40] L. Kong, Y. Tian, and Z.-H. Zhang, Defects in the 3-dimensional toric code model form a braided fusion 2-category, *J. High Energy Phys.* **12** (2020) 078.
- [41] J. Haah, Local stabilizer codes in three dimensions without string logical operators, *Phys. Rev. A* **83**, 042330 (2011).
- [42] S. Vijay, J. Haah, and L. Fu, A new kind of topological quantum order: A dimensional hierarchy of quasiparticles built from stationary excitations, *Phys. Rev. B* **92**, 235136 (2015).
- [43] M. Mühlhauser, M. R. Walther, D. A. Reiss, and K. P. Schmidt, Quantum robustness of fracton phases, *Phys. Rev. B* **101**, 054426 (2020).
- [44] C. Zhou, M.-Y. Li, Z. Yan, P. Ye, and Z. Y. Meng, Evolution of dynamical signature in the X-cube fracton topological order, *Phys. Rev. Res.* **4**, 033111 (2022).
- [45] G.-Y. Zhu, J.-Y. Chen, P. Ye, and S. Trebst, Topological fracton quantum phase transitions by tuning exact tensor network states, [arXiv:2203.00015](https://arxiv.org/abs/2203.00015).
- [46] G. Evenbly and G. Vidal, Scaling of entanglement entropy in the (branching) multiscale entanglement renormalization ansatz, *Phys. Rev. B* **89**, 235113 (2014).
- [47] G. Evenbly and G. Vidal, Tensor network states and geometry, *J. Stat. Phys.* **145**, 891 (2011).
- [48] B. Swingle, Entanglement renormalization and holography, *Phys. Rev. D* **86**, 065007 (2012).
- [49] G. Evenbly, Hyperinvariant Tensor Networks and Holography, *Phys. Rev. Lett.* **119**, 141602 (2017).